

# Nonmonotonic Pair Potentials in the Interaction of Like-Charged Objects in Solution

Ali Behjatian, Rowan Walker-Gibbons, Alexander A. Schekochihin, and Madhavi Krishnan\*



Cite This: *Langmuir* 2022, 38, 786–800



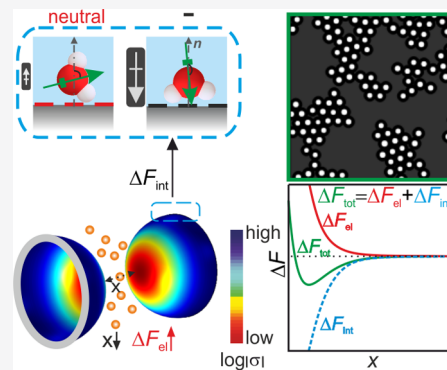
Read Online

ACCESS |

Metrics & More

Article Recommendations

**ABSTRACT:** We consider the long-standing like-charge attraction problem, wherein under certain conditions, similarly charged spheres suspended in aqueous electrolyte have been observed to display a minimum in their interaction potential, contrary to the intuitively expected monotonically varying repulsion. Recently, we described an interfacial mechanism invoking the molecular nature of the solvent that explains this anomalous experimental observation. In our model for the interaction of negatively charged particles in water, the minimum in the pair potential results from the superposition of competing contributions to the total free energy. One of these contributions is the canonical repulsive electrostatic term, whereas the other is a solvation-induced attractive contribution. We find that whereas both contributions grow approximately exponentially with decreasing interparticle separation, the occurrence of a stable, long-ranged minimum in the pair potential arises from differences in the precise interparticle separation dependence of the two terms. Specifically, the interfacial solvation term exhibits a more gradual decay with distance than the electrostatic repulsion, permitting the attractive contribution to dominate the interaction at large distances. Importantly, these disparities become evident in quantities calculated from exact numerical solutions to the governing nonlinear Poisson–Boltzmann (PB) equation for the spatial electrical potential distribution in the system. In marked contrast, we find that the linearized PB equation, applicable in the regime of low surface electrical potentials, does not support nonmonotonic trends in the total interaction free energy within the present model. Our results point to the importance of exact descriptions of electrostatic interactions in real systems that most often do not subscribe to particular mathematical limits where analytical approximations may provide a sufficiently accurate description of the problem.



## 1. INTRODUCTION

Many natural processes involve the complex interplay of interactions between particles, molecules, and molecular-scale entities in the solution phase. At the heart of the rich collective behavior on the macroscopic scale lies the pairwise interaction of particles or molecular-scale entities in isolation. Great strides have been made in establishing the theoretical basis of these interactions, and our understanding of interparticle behavior in solution is by and large thought to be complete. However, there exist important anomalous experimental observations in the literature, explanations for which have persistently remained outside the scope of the existing theoretical framework. One such problem concerns the repeated, counterintuitive experimental observation of attraction between like-charged objects in aqueous solution under conditions that constitute the regime of weak electrostatic coupling, where Poisson–Boltzmann (PB) theory is expected to apply.<sup>1,2</sup>

We consider the interaction of two identical like-charged spheres in an aqueous electrolyte containing exclusively monovalent salt at low ionic strength. In low concentrations of monovalent salt ( $c_0 < 1$  mM), PB theory provides an accurate description of electrostatic interactions and generally predicts a

monotonically increasing repulsion with decreasing interparticle separation.<sup>1,3</sup> Over the past several decades, however, several independent studies have reported long-range attractive interactions between like-charged dielectric entities in low ionic strength solution. These observations depart qualitatively from the PB picture.<sup>4–17</sup> Specifically, the interaction free energy for like-charged particles is generally expected to increase with decreasing particle separation. The experiments reveal, however, that the free energy of interaction decreases with decreasing separation at long range, goes through a minimum, and then increases with decreasing separation at shorter range, as expected. The presence of a shallow yet non-negligible minimum of depth  $\gtrsim 1k_B T$  in the pair interaction implies the formation of stable, reorganizing clusters composed of particles

**Received:** October 22, 2021

**Revised:** December 9, 2021

**Published:** January 4, 2022



that should by all accounts repel at all distances.<sup>12,15,18</sup> Note that under the relevant experimental conditions, corrections such as those arising from ion correlations, finite ion size, and charge density fluctuations are not sufficient to render the screened repulsion attractive at long range.<sup>19–21</sup> We further point out that although some studies have suggested that the observed attraction requires the presence of confining walls,<sup>22,23</sup> other investigations provide evidence of the long-ranged interparticle attraction between an isolated pair of particles in bulk solution.<sup>14</sup> Finally, although some of the experimental reports have come under scrutiny for measurement artifacts,<sup>24,25</sup> the overall observation has thus far evaded satisfactory explanation and continues to attract both theoretical and experimental interest.<sup>14,15,26,27</sup>

The body of like-charge attraction experiments that we address in this work concerns measurements performed at thermal equilibrium by the direct observation of interparticle interactions in solution using optical microscopy. The system properties measured are pair-interaction potentials or pair-potential-governed behavior such as radial distribution functions,  $g(r)$ . Optical microscopy offers sensitive measurements of interaction energies smaller than the thermal energy scale,  $k_B T$ , where  $k_B$  is Boltzmann's constant and  $T$  is the absolute temperature, fostering accurate measurement of interparticle forces in the femtonewton regime.<sup>28</sup> The pair-potential measurements that we refer to all had one feature in common: They displayed a minimum in the interparticle interaction energy at extremely large intersurface separations, generally  $5–10\kappa^{-1}$ . The Debye length,  $\kappa^{-1} = \sqrt{\epsilon_0 \epsilon_r k_B T / \sum_i z_i^2 N_A c_{i,0} e^2}$ , is a length scale characterizing the exponential spatial screening of the electrical potential at a charged surface by a cloud of oppositely charged counterions in solution. Here  $e$ ,  $\epsilon_0$ ,  $\epsilon_r$ ,  $c_{i,0}$ ,  $N_A$ , and  $z_i$  are the elementary charge, permittivity of free space, relative permittivity of the aqueous medium, bulk ion concentration, Avogadro's number, and valence of the  $i$ th ionic species in solution, respectively. Given that  $\kappa^{-1} \approx 95$  nm in a solution containing monovalent ions at a concentration of  $c_0 = 10 \mu\text{M}$ , the measured location of the minimum in the experiments was generally in the range of 0.5 to 2  $\mu\text{m}$ .<sup>9,14,15,29,29</sup>

Much effort has been devoted to deducing the mechanism underlying the anomalous observed attraction. Arguably, the main challenge has revolved around explaining how the screened electrostatic interaction might result in a measurable attraction at interparticle separations so large that an exponentially damped perturbation ought to have died out entirely. To meet this exacting requirement, one heuristic explanation for experimental observations on particles confined between parallel plates invoked a space charge of opposite sign midway between the two charged particles.<sup>14,30</sup> Thus, in addition to the canonical screened electrostatic repulsion, each particle was thought to interact with a space charge, positioned midway between the particles, via a screened Coulombic interaction that provided the required attractive contribution to the total force. The proposed phenomenological total interaction potential was thus of the form  $U(r) = a \exp(-\kappa r)/r - b \exp(-\kappa r/2)/r$ , where  $a$  and  $b$  are positive constants and  $r$  is the center-to-center particle separation. Here the first term reflected the traditional electrostatic repulsion, and the second, Yukawa-like term represented the attraction whose origin was yet to be rigorously understood. The basic proposal, however, reflected arguments along the lines of those outlined in refs 4 and 26. Interestingly,

the second term in the proposed pair potential may be viewed as a screened Coulombic interparticle attraction that decays spatially at a rate given by twice the Debye length.

We recently proposed a theoretical framework that explains key features of the like-charge attraction observations and does so in a quantitative fashion for different sets of experiments, covering an order of magnitude in particle size and a broad range of experimental conditions.<sup>31</sup> In our model, the response of interfacial solvent molecules at an electrically charged surface makes a separation-dependent contribution to the total free energy of interaction of the two particles, which often results in a long-ranged, attractive contribution to the total force. Here we show that the interfacial contribution has an interparticle separation dependence that is different from that of the electrostatic repulsion. This difference in separation dependence results in a free-energy minimum at large interparticle separations. We emphasize that in our model, the response of interfacial water is limited to the equivalent of the first two or three hydration shells, the region in the immediate vicinity (within  $\sim 0.5$  nm) of the solid–liquid interface, as observed in molecular dynamics (MD) simulations and in interfacial spectroscopy experiments.<sup>31–34</sup> The long-range contribution of interfacial water to the total free energy in our model comes about purely as a result of the long-range nature of the screened electrostatic interaction in solution. The model does not invoke any longer-range orientational order of water reported to occur at distances  $>1$  nm around ions in electrolyte solutions.<sup>35,36</sup>

## 2. METHODS

We begin by summarizing the central elements of our theoretical model for the interaction of like-charged particles in solution. We consider two hollow spherical particles of radius  $R$  whose centers are separated by a distance  $r = 2R + x$  immersed in an electrolyte containing only monovalent ionic species at a concentration  $c_0$ . We use the framework of the PB-equation-based approach for calculating electrostatic interaction free energies for charged objects in solution.<sup>37–39</sup> The nonlinear PB (NLPB) equation

$$\nabla^2 \psi(\mathbf{r}) = \kappa^2 \sinh \psi(\mathbf{r}) \quad (1)$$

for the dimensionless electrical potential,  $\psi(\mathbf{r}) = e\phi(\mathbf{r})/k_B T$ , in solution can be solved using various boundary conditions on the particle surface, namely, the constant electrical charge, constant potential, and charge regulation. In our work, we use the charge regulation boundary condition at the surface of the spheres, as it most closely resembles experimental reality.<sup>40–42</sup> Here the charge density at a point,  $\mathbf{R}$ , on the surface of the particle is given by

$$\sigma(\mathbf{R}) = z\alpha(\mathbf{R})\Gamma e \quad (2)$$

where

$$\alpha(\mathbf{R}) = 1/[1 + 10^p \exp(z\psi(\mathbf{R}))] \quad (3)$$

with  $p = z(\text{pH} - \text{p}K)$ . In the above equations,  $\alpha(\mathbf{R})$  denotes the ionization probability of a surface group of valence,  $z$ , in the ionized state,  $\Gamma$  is the density of ionizable surface groups,  $\text{p}K$  is the negative decadic logarithm of the group's ionization equilibrium constant, and  $\text{pH}$  reflects that of the hydronium ion concentration in bulk solution. Note that in this work, we only consider a single species of the anionic surface group. Solving eq 1 subject to the boundary condition in eqs 2 and 3 gives the spatial distribution of  $\psi(\mathbf{r})$  and the regulated surface charge density,  $\sigma(\mathbf{R})$ , on the charged surfaces.  $\psi(\mathbf{R})$  is the corresponding surface electrical potential, denoted hereafter by  $\psi_s$ . Note that as  $p \rightarrow -\infty$  we have  $\alpha \rightarrow 1$ , which implies that the surfaces remain essentially at constant charge  $\sigma = z\alpha\Gamma e$  at all separations,  $x$ . This condition is to be contrasted with a situation where  $10^p \exp(z\psi_s) \rightarrow 1$ , where  $\alpha \rightarrow 0.5$  and the effect of charge regulation is substantial. The electrostatic free energy,  $\Delta F_{el}(x)$ , at any interparticle separation,  $x$ , is

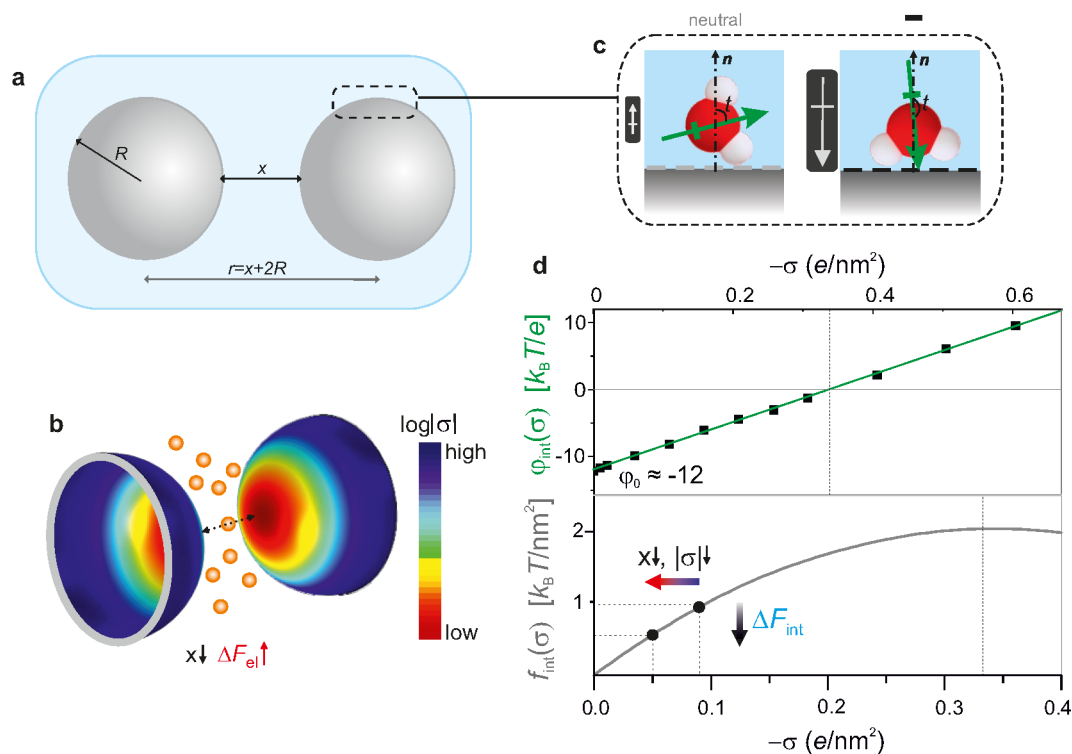


**Figure 1.** Solvation at an interface plays a role in the interaction between electrically charged objects in solution. (a) Schematic depiction of two identical, charged spherical particles of radius  $R$  whose centers are separated by  $r = x + 2R$ , where  $x$  denotes the minimum intersurface separation between the particles. (b) Charge density,  $\sigma$ , on the surface of the particles at a separation  $x$  depicting a reduction in magnitude of  $\sigma$  on the regions of the sphere surfaces at closest approach. This is a result of charge regulation of the ionizable surface groups. Compression of the counterions in the gap (orange spheres, not to scale) gives rise to an entropically governed repulsive force that generally increases with decreasing separation. Reproduced from ref 31, with the permission of AIP Publishing. (c) Schematic depiction of a water molecule at the interface of the particle with aqueous solution. Configurations shown illustrate the average orientation of interfacial water molecules at surfaces carrying a strongly negative charge (right) and no charge (left), as inferred from molecular dynamics (MD) simulations.  $t$  denotes the angle included between the molecular dipole moment (green) and the outward-directed surface normal,  $\mathbf{n}$  (dashed line). As the surface charge changes from zero to strongly negative, there is an inversion in the average orientation of interfacial water. (d) This progressive inversion, or flipping, of the average orientation vector of water molecules is associated with an interfacial potential,  $\varphi_{\text{int}}(\sigma)$ , that varies in both sign and magnitude as a function of charge density,  $\sigma$  (ref 31) (top panel). The integral  $f_{\text{int}}(\sigma) = \int_0^\sigma \varphi_{\text{int}}(\sigma) d\sigma$  relates  $\varphi_{\text{int}}(\sigma)$ , extracted from MD simulations, to the excess interfacial hydration free energy per unit area of surface,  $f_{\text{int}}(\sigma)$  (bottom panel). We obtain  $\varphi_{\text{int}}(\sigma = 0) = \varphi_0 \approx -12k_B T/e$  for water at a model interface, which entails an increase in interfacial free energy with increasing magnitude of  $\sigma$  in the regime of low negative charge density,  $|\sigma| < 0.4e/\text{nm}^2$ . This, in turn, implies a reduction in total interfacial solvation free energy,  $\Delta F_{\text{int}}$ , with decreasing interparticle separation, which acts to offset the counterion-mediated electrostatic repulsion,  $\Delta F_{\text{el}}$ , depicted in panel b.

determined using the appropriate free-energy functional, as described previously.<sup>31,38,39</sup>

We then go beyond the continuum-electrostatics picture by including the response of interfacial water in the calculation of the distance-dependent free energy. Specifically, we consider the contribution to the potential of mean force arising from the response of molecular water to the distance-dependent regulation (alteration) of the electrical charge on the particle surface. This molecular-level contribution entails a component arising from symmetry breaking at the interface which is generally absent from continuum theories that regard the solvent as a smooth featureless medium.

The mechanism behind the response of molecular water to a changing electrical charge density on a surface immersed in solution and the calculation of the associated free energy have been described in detail in previous work.<sup>31</sup> In brief, the water molecule can be viewed as a dipole whose average orientation at an interface is a function of the sign and magnitude of the electrical charge density at the surface in solution, giving rise to the solvation free energy.<sup>31–34,43,44</sup> When two objects carrying ionizable surface groups approach each other, it is well known that the groups regulate their charge in such a manner as to minimize the total free energy of the system. In general, this behavior entails a reduction in magnitude of charge upon the approach of two similarly charged objects, and the average orientation of interfacial water

molecules is expected to be altered in response.<sup>40</sup> Interestingly, both molecular simulations and spectroscopy experiments have revealed that even at an uncharged surface, water has a slight preferential, or anisotropic, orientation on average, which is thought to arise from more favorable hydrogen bonding to the bulk<sup>31,33,34,45,46</sup> (Figure 1c). This anisotropy in the orientation of interfacial water molecules gives rise to an excess electrical potential at the surface,  $\varphi_{\text{int}}$ . This excess interfacial potential, or the solvation potential, is related to an excess interfacial hydration free energy per unit area of surface,  $f_{\text{int}}(\sigma)$ , via the integral  $f_{\text{int}}(\sigma) = \int_0^\sigma \varphi_{\text{int}}(\sigma) d\sigma$  (refs 31 and 32) (Figure 1d). We have performed MD simulations of water at model interfaces and found that the excess hydration free energy has a pronounced nonmonotonic character as a function of the surface charge density,  $\sigma$ , for negatively charged surfaces. Such behavior has, in fact, not only been found for spherical cavities representing ions, for which the nonmonotonic trend was originally noted but also holds for 2D surfaces in solution.<sup>31,32,46</sup> Importantly, the contribution from this excess hydration free energy to the total free energy of interaction between two particles is not accounted for within the continuum picture<sup>31</sup> (Figure 1d). The anisotropy in the orientation of water at an uncharged surface can be seen as another manifestation of a solvent-generated charge-asymmetry effect resulting from the bent-core structure of water. An arguably better

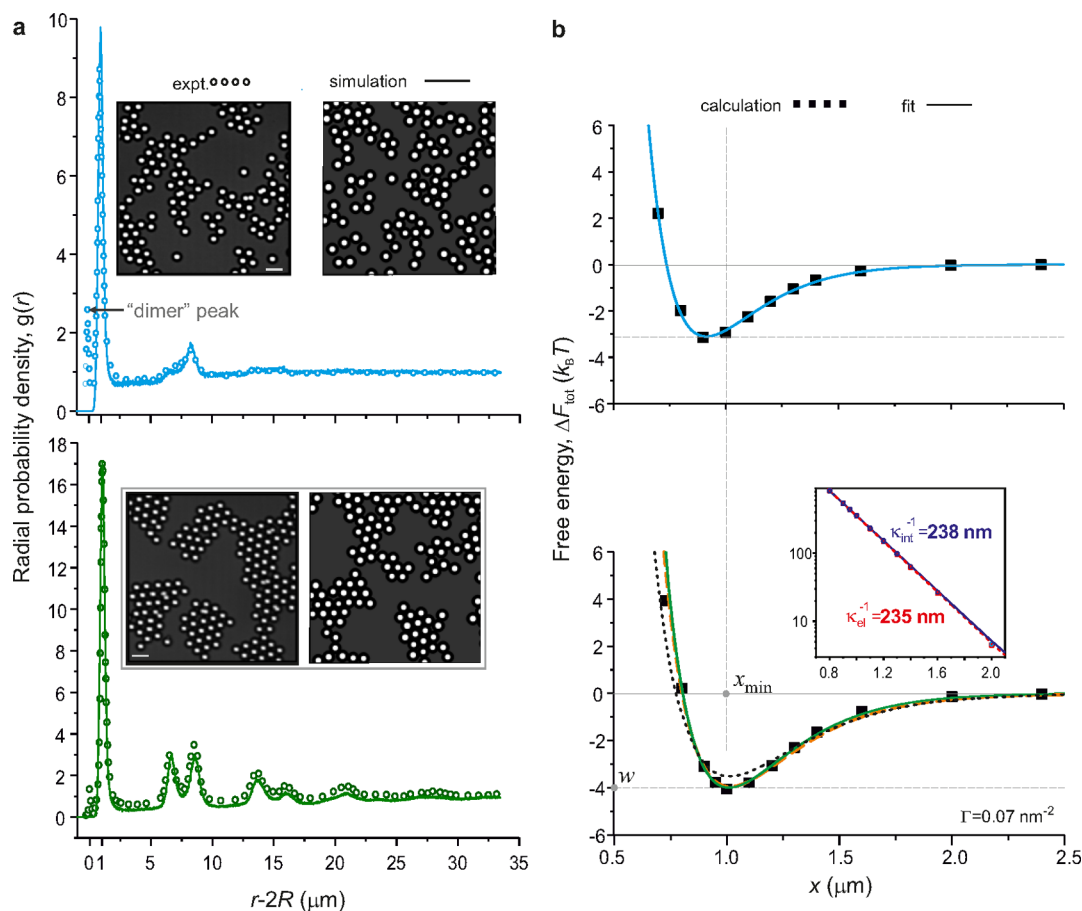


**Figure 2.** Comparison of the predictions of the interfacial hydration model with experimental measurements taken from ref 15. (a) Experimentally measured radial probability density functions,  $g(r)$  (open circles), and theoretically predicted  $g(r)$  curves from our model (solid lines) for silica particles coated with lipid bilayers containing two different net densities of negatively charged lipids,  $\Gamma = 0.014 \text{ nm}^{-2}$  corresponding to 1 mol % negative lipids (top) and  $\Gamma = 0.07 \text{ nm}^{-2}$  corresponding to 5 mol % negative lipids (bottom). Insets present microscopy images from experiments (left) and corresponding Monte Carlo (MC) simulation snapshots (right). Scale bars denote  $10 \mu\text{m}$ . Experimental images correspond to cases referred to in ref 15 as  $-37$  (top) and  $-55$  mV (bottom). Reproduced with permission from ref 15. Copyright 2009 Royal Society of Chemistry. (b) Calculated pair interaction potentials (symbols) for two sets of experimental conditions: Top panel:  $\Gamma = 0.014 \text{ nm}^{-2}$ ,  $c_0 = 2.16 \mu\text{M}$ ,  $p = -2.201$ . The data are overlaid with the function  $\Delta F_{\text{tot}}/k_B T = A \exp(-\kappa_1 x) + B \exp(-\kappa_2 x)$  (eq 5), where  $A = 6902$ ,  $B = -5000$ ,  $\kappa_1^{-1} = 169.5 \text{ nm}$ , and  $\kappa_2^{-1} = 183.65 \text{ nm}$ . Bottom panel:  $\Gamma = 0.07 \text{ nm}^{-2}$ ,  $c_0 = 1.66 \mu\text{M}$ ,  $p = -1.521$ . The curve corresponds to eq 5 with parameter values  $A = 11\,093$ ,  $B = -9152$ ,  $\kappa_1^{-1} = 204 \text{ nm}$ , and  $\kappa_2^{-1} = 214.6 \text{ nm}$ . These pair-potential fit functions served as inputs to the MC simulation to generate the particle configurations and corresponding  $g(r)$  values presented in panel a. For comparison, alternate sets of pair-potential parameters also describe the calculated interaction energy data well: [1]  $\kappa_1^{-1} = 180 \text{ nm}$ ,  $\kappa_2^{-1} = 254 \text{ nm}$ ,  $A = 2708$ , and  $B = -740$  (orange dashed curve) and [2]  $\kappa_1^{-1} = \kappa_{\text{el}}^{-1} = 235.4 \pm 0.3 \text{ nm}$ ,  $\kappa_2^{-1} = \kappa_{\text{int}}^{-1} = 237.9 \pm 0.3 \text{ nm}$ ,  $A = 24\,630$ , and  $B = -23\,780$  (black dotted curve and inset).

known phenomenon along similar lines is the strong preferential solvation of anions over cations in water.<sup>32,47–49</sup>

We point out that in our MD simulations, the charged walls were modeled using a lattice of oxygen atoms, as described in ref 31, but studies on water orientation at silica, alumina, and polystyrene surfaces indicate trends that are in qualitative agreement with these results.<sup>50–52</sup> Nonetheless, hydration at an aqueous bilayer interface where the lipid head groups bear both positive and negative ionized moieties is undoubtedly more complex than that at an oxygen atom or silica interface. It is also possible that in the composite interfacial system of the experiment considered here, the response of the hydrated silica surface underlying the lipid bilayer contributes strongly to the overall behavior.<sup>15</sup> For the purpose of this work, however, we assume that the qualitative trend for the excess hydration free energy at the lipid bilayer–silica particle interface is similar to the result obtained for the O-atom wall system, shown in Figure 1d.

Furthermore, it is worth noting here that the nonmonotonic trend in interfacial free energy in Figure 1d relies on an excess interfacial potential at an uncharged surface of  $\phi_0 \approx -0.3 \text{ V}$  calculated with respect

to the bulk liquid.<sup>31</sup> Referencing the potential to the wall interior rather than the bulk liquid would give an interfacial potential of the opposite sign, namely, ca.  $+0.3 \text{ V}$ , where the positive sign agrees with the potential of about  $+3.5 \text{ V}$  calculated from the quantum-mechanical charge distribution using density functional theory (DFT).<sup>53</sup> It is well known that unrestricted spatial averaging of the electrical potential in DFT may not reflect the value of the electrical potential felt by ions and ionized groups that reside in the interstitial spaces between water molecules in solution.<sup>53,54</sup> Indeed, some indirect electrochemical estimates of the interfacial potential place its value at about  $+0.1 \text{ V}$  with respect to vacuum, which is in qualitative agreement with our calculated value of approximately  $+0.3 \text{ V}$  for the simple point charge (SPC) water model.<sup>54,55</sup> Note that we consider only the dipolar contribution of the modeled molecular charge distribution to the interfacial potential.<sup>32,54</sup> Inclusion of the quadrupolar moment of SPC water models can change the sign of the calculated interfacial potential to about  $-0.5 \text{ V}$  with respect to vacuum.<sup>56</sup> However, prior theoretical arguments question the physical validity of such a result.<sup>32,54,57</sup>

To obtain the total interparticle interaction free energy as a function of intersurface separation,  $x$ , to the first approximation, we simply add the interfacial hydration free energy,  $\Delta F_{\text{int}}$ , to the PB electrostatic free energy,  $\Delta F_{\text{el}}$  (ref 31). The total free energy,  $\Delta F_{\text{tot}} = \Delta F_{\text{el}} + \Delta F_{\text{int}}$ , in our model thus has two key ingredients: (1) the electrostatic free energy from a charge-regulated interaction, which has been well described previously, and (2) the orientational response of interfacial molecular water to a changing electrical charge density on the approaching particles. The free energy of the former process,  $\Delta F_{\text{el}}$ , can be calculated in a straightforward fashion using mean-field PB theory.<sup>31,38,39</sup> We determine the contribution from the latter mechanism,  $\Delta F_{\text{int}}$ , by obtaining the interfacial hydration free energy per unit area,  $f(\sigma)$ , from molecular simulations and evaluating the integral

$$\Delta F_{\text{int}}(x) = \int_S \Delta f(\sigma(\mathbf{R}); x) \, dA \quad (4)$$

over all charged surfaces,  $S$ , as described in previous work.<sup>31</sup>

Throughout this work  $\Delta$  denotes differences in the quantity with respect to the value at infinite separation. In general, the electrostatic contribution is always monotonically repulsive for realistic experimental conditions, where particles always retain a net electrical charge of the same sign.<sup>58</sup> In slightly different terms, as long as a particle's ionized groups do not discharge entirely or change sign upon encountering a nominally identical neighbor, the electrostatic free energy of interaction,  $\Delta F_{\text{el}}$ , generally always implies a repulsive force, especially at the longer range,  $x > \kappa^{-1}$ . In contrast, the interfacial contribution to the total free energy can give rise to either a monotonically attractive or repulsive force with decreasing interparticle distance.

In summary, two approaching like-charged particles will generally experience a reduction in surface charge. The electrostatic free energy of the interaction will remain positive and increasing, as the particles retain a substantial net electrical charge of the same sign. But the interfacial free energy, which changes due to the reduction in surface charge density, as shown in Figure 1d, provides an additional contribution to the total free energy. Depending on the magnitude of the net electrical charge on the surface of each particle in isolation, this contribution to the free energy may turn out to either increase or decrease with interparticle separation for two identical objects. Ref 31 shows that for materials carrying anionic ionizable groups immersed in aqueous electrolytes of pH close to the pK of their ionizable groups, an attractive interfacial contribution to the total free energy is expected to be the norm rather than the exception.

**2.1. Experimental System of Interest.** In this work, we focus on recent experiments of Groves et al., who used fluorescence microscopy to measure radial probability density distributions in a 2D system of colloidal particles suspended in aqueous electrolyte.<sup>12,15,18</sup> In brief, the experiments in ref 15 were conducted using  $R = 3.25 \mu\text{m}$  silica particles coated with lipid bilayers of tunable electrical charge composition. In low ionic strength solution of  $c_0 \approx 5 \mu\text{M}$ , nominally repulsive like-charged particles were counterintuitively observed to form large, stable, slowly reorganizing clusters, indicative of an attractive interparticle interaction. The formation and dissolution of clusters was found to be very sensitive to the ionic strength in solution, and the observed interparticle spacing in the clusters suggested a minimum in the pairwise interaction potential at an intersurface separation,  $x \approx 1 \mu\text{m}$  (Figure 2).<sup>15</sup> The pH of the solution is assumed to be 5.5, corresponding to that of deionized water equilibrated with air. The study examined particles with various surface chemistries, including silica, similar to ref 30, polystyrenesulfonate, similar to ref 9, and charged lipid bilayers, and the same qualitative behavior was found in all cases.<sup>15</sup>

We set out to compare the experimentally measured radial probability density functions for particle distributions,  $g(r)$ , reported in ref 15, with calculations from our theoretical model. To do so, in the theoretical calculation, we held constant the particle radius,  $R$ , and the surface ionizable group density,  $\Gamma$ . We varied the parameters,  $p = z(\text{pH} - \text{pK})$  and  $c_0$ , and generated various pair potentials, as described previously.<sup>31</sup> We then fed the calculated pair potential as an input to a Monte Carlo (MC) simulation of an ensemble of particles in a 2D box

and generated simulated  $g(r)$  profiles for comparison with measurements. Note that in the MC simulation, we include a particle-size dispersion of 4%, as quoted in the experimental study. Performing this procedure iteratively permits us to determine a set of parameters describing the particle–electrolyte system that yields simulated  $g(r)$  profiles that are in good agreement with the measurements. We emphasize here that we have assumed that interactions in the experimental 2D ensemble of particles can be regarded as pairwise additive. Studies on silica particles in the regime of  $\kappa R \approx 2$  have shown that the repulsive interaction between a pair of particles is modified by the presence of a third particle in close proximity.<sup>59</sup> In the experiments considered in this study, the particle size,  $\kappa R \gtrsim 14$ , and the interparticle separation range of interest,  $\kappa x \gtrsim 5$ , are both large compared with the Debye length. We therefore assume in this study that the collective behavior of an ensemble of particles can be approximated by pairwise additive interactions.

Obtaining good agreement between the simulated and observed  $g(r)$  profiles entailed matching the depth of the minimum in the calculated pair potential to within 3% and its location to within about 5% of the experimentally observed values. We point out that with  $\Gamma$ ,  $c_0$ , and  $R$  held constant, the value of  $p$  had to be fine-tuned to the third decimal place to obtain  $g(r)$  functions that best fit the experimental data. Note that whereas the MC model includes the experimental particle size dispersion, the theoretical calculation for the pair potential assumes a fixed particle size. The calculation further excludes temporal fluctuations in quantities such as the salt concentration and pH, inherent in data acquisition performed over experimental time scales. Therefore, the fine-tuning of  $p$  in this exercise should be viewed in the context of accounting for a myriad small experimental fluctuations using a single tunable parameter. The quoted values for  $p$  should not be interpreted, for instance, as a requirement for experimental pH stability down to  $10^{-3}$  units, which would be impossible to meet in practice. We point out that any other parameter or sets of parameters may also be fine-tuned to obtain agreement because there is always a degree of uncertainty in quoted values of  $c_0$ ,  $\Gamma$ , and so on in experimental data.

The values of  $p$  from our analysis imply pK values for the ionizable surface groups ranging from 3.3 to 4, which are in agreement with values reported in the literature both for phosphate head groups in lipid bilayers and for acidic ionizable surface groups on silica.<sup>31,60–62</sup> The obtained values of pK are, however, estimates based on the particular  $f(\sigma)$  function used, which may change upon the inclusion of molecular detail describing the lipid bilayer. The calculation of a more exact  $f(\sigma)$  function from a full molecular simulation of the aqueous interface at the lipid bilayer–silica particle surface, accounting for the exact composition and chemistry of lipids in the experiment and potentially including the detail of the underlying bilayer–silica interface, is beyond the scope of this work.<sup>63</sup>

Having established the ability to obtain quantitative agreement between the theoretical model and the experimental study for reasonable values of all system parameters, we examine the origin of the minimum in the total interaction potential for a pair of like-charged particles in water.

**2.2. Examining the Separation Dependence of the Interfacial Hydration Contribution.** We recognize that, just like the repulsive electrostatic contribution, the attractive contribution to the pair potential is fundamentally dependent on the screened electrostatic response (as described in detail later in this section). Therefore, at first glance, we expect the distance dependence of both contributions to be described by exponential functions with the same screening length parameter, given by the Debye length,  $\kappa^{-1}$ . But superposition of exponentially varying attractive and repulsive contributions described by the same screening length parameter always yields a result that is itself either zero everywhere or monotonic in nature—either attractive or repulsive. Such behavior precludes the appearance of a minimum at any interparticle separation. However, we found that under specific conditions determined by the pH, pK, ionic strength, and surface group density, our calculations of distance-dependent interaction free energies for a pair of particles in solution revealed a long-range minimum at  $x \approx 5\kappa^{-1}$ . Thus at long range ( $R > x \gtrsim 2\kappa^{-1}$ ), calculations for large spheres

( $R \gg \kappa^{-1}$ ) revealed a total interaction potential given by the sum of two terms, of the form

$$\Delta F_{\text{tot}}(x) = A \exp(-\kappa_1 x) + B \exp(-\kappa_2 x) \quad (5)$$

with  $A > 0$ . Here the first term represents the overall repulsive electrical free energy,  $\Delta F_{\text{el}} = A \exp(-\kappa_{\text{el}} x)$ , and the second term,  $\Delta F_{\text{int}} = B \exp(-\kappa_{\text{int}} x)$ , denotes the contribution from the interfacial hydration mechanism, which implies an attractive contribution to  $F_{\text{tot}}$  when  $B < 0$ . Note that for the electrostatic free energy,  $\Delta F_{\text{el}}$ , we do not use the traditional screened Coulombic form, that is,  $\exp(-\kappa r)/r$ , generally applied to spheres at a center-to-center separation,  $r$ . In this work,  $R \gg \kappa^{-1}$ , which represents the thin double-layer limit, and we consider the range  $R > x > \kappa^{-1}$ , where  $r$  varies about 10–20% over the entire range of  $x$  considered. Fitting a screened Coulomb function to the calculated repulsive free energy,  $\Delta F_{\text{el}}$ , for example, results in screening lengths  $\sim 3\%$  larger than those for a simple exponential. This discrepancy is much smaller than the uncertainty in nominal salt concentration in experiments, and the fitting procedure itself involves uncertainties including treating the amplitude of the decay as a free parameter. Furthermore, the screened Coulombic form makes a noticeable contribution for  $x \gtrsim R$ . Because  $R \gg \kappa^{-1}$  in this study, the regime is not meaningfully probed in the problem, rendering the simple exponential,  $\Delta F_{\text{el}} = A \exp(-\kappa_{\text{el}} x)$ , a sufficient description. We have also ignored the van der Waals (vdW) contribution to the total interaction potential because it is negligible over the interparticle separation range of interest. For example, at an interparticle separation of  $x = 0.5 \mu\text{m}$ , the vdW contribution to the total interaction free energy is  $\Delta F_{\text{vdw}} \approx -0.1 k_{\text{B}} T$  for the experimental system in Figure 2.

Although the repulsive electrostatic and attractive interfacial terms each displayed an exponentially varying spatial dependence, importantly, we found that the screening lengths for the two contributions were slightly different. We deliberately use parameters  $\kappa_1$  and  $\kappa_2$  in place of  $\kappa_{\text{el}}$  and  $\kappa_{\text{int}}$  in eq 5, as the latter pair of values represents quantities determined using the calculated free energies, which are likely to be *a priori* unknown for an experimental system under study. Values for  $\kappa_1$  and  $\kappa_2$  could be obtained, for instance, from fits of eq 5 to the experimentally measured total potential. Importantly, the values for  $\kappa_1$  and  $\kappa_2$  obtained from such a fit, in conjunction with the corresponding values for  $A$  and  $B$ , need not turn out to be exactly the same as the corresponding quantities  $\kappa_{\text{el}}$  and  $\kappa_{\text{int}}$ , which are obtained from fits to the calculated free energies. (See Figure 2b.)

Further exploring the properties of the pair potential, we found that the attractive interfacial contribution was best described by a screening length that is of comparable magnitude but, importantly, always slightly larger than that governing the electrostatic interaction free energy, that is,  $\kappa_{\text{int}}^{-1} > \kappa_{\text{el}}^{-1}$ . For instance, in the example that we focus on, presented in Figure 2a,  $\kappa_{\text{el}}^{-1} = 235 \text{ nm}$  and  $\kappa_{\text{int}}^{-1} = 238 \text{ nm}$ , but good fits may be obtained for different values of the screening lengths, for example,  $\kappa_1^{-1} = 204 \text{ nm}$  and  $\kappa_2^{-1} = 215 \text{ nm}$ . Importantly, we find that when the interaction potential reveals a long-range minimum, the following conditions hold:  $\kappa_{\text{int}} < \kappa_{\text{el}}$  and  $A > |B|$ . We proceed to explore the origin of the observed larger screening length for the attractive part of the interaction. We show that it arises from the solution of the NLPB equation for the electrical potential in the system of two approaching charged spheres, where the linear regime governed by  $\psi_s \ll 1$  does not rigorously apply.

To facilitate the analysis, we first provide a simple expression for the interfacial free energy difference,  $\Delta F_{\text{int}}$ , arising from the response of interfacial water to charge regulation on the particle surface. Solving the PB equation gives the electrical potential,  $\psi(\mathbf{r})$ , as a function of position in the entire particle–electrolyte system. Therefore, the regulated charge density,  $\sigma$ , on the particle surface is determined self-consistently by eq 2. Subsequently, the corresponding interfacial hydration contribution is readily deduced from either the  $f(\sigma)$  or  $\varphi_{\text{int}}(\sigma)$  result obtained from MD (Figure 1d), described as follows.

In the interaction of two approaching flat surfaces at a separation  $x$ , the change in interfacial solvent free energy per unit area,  $\Delta f_{\text{int}}$ , with respect to the value at infinite separation at a location  $\theta$  on the sphere surface may be written as

$$\begin{aligned} \Delta f_{\text{int}}(\theta; x) &= \int_{\sigma(\theta; \infty)}^{\sigma(\theta; x)} \varphi_{\text{int}}(\sigma) d\sigma \\ &= z e \int_{\psi_{s, \infty}}^{\psi_s(\theta; x)} \varphi_{\text{int}}(\psi_s) \Gamma \frac{d\alpha}{d\psi} d\psi_s(\theta; x) \end{aligned} \quad (6)$$

where we implicitly invoke eqs 2 and 3 relating  $\sigma$  and  $\psi_s$ . For very small changes in  $\psi_s(\theta; x)$  such that  $\psi_s(\theta; x) \approx \psi_{s, \infty}$ , which holds at large interparticle separations,  $\kappa x \gtrsim 2$ , we may make the approximation

$$\Delta f_{\text{int}}(\theta; x) \approx z e \varphi_{\text{int}}(\psi_{s, \infty}) \Gamma \frac{d\alpha}{d\psi} \Big|_{\psi_{s, \infty}} \Delta \psi_s(\theta; x) \quad (7)$$

where  $z$  is the valence of the ionized surface group and takes the value  $-1$  or  $+1$  for monovalent anionic or cationic groups, respectively. Next,  $\varphi_{\text{int}} = \varphi_0 + k\sigma$  is the interfacial potential or solvation potential at an interface as a function of the surface charge density,  $\sigma$ , as shown in Figure 1, and is obtained from MD simulations of water, described in ref 31. Furthermore, considering only monovalent ionizable sites where  $z^2 = 1$ , we have

$$z \frac{d\alpha}{d\psi} = \frac{-10^p \exp(z\psi_s)}{[1 + 10^p \exp(z\psi_s)]^2} = -[1 - \alpha(\psi_s)] \alpha'(\psi_s) \quad (8)$$

from eq 3, the relationship governing the charge regulation of the surface ionizable groups. Note that when  $10^p \exp(z\psi_s) \approx 1$ , charge regulation of the surface groups is maximal, implying  $z d\alpha/d\psi_s = -0.25$ . In turn,  $\Delta \psi_s = \psi_s(\theta; x) - \psi_{s, \infty}$  is the infinitesimal perturbation in electrical potential at any point  $\theta$  on the surface of the sphere due to the approach of another charged object relative to the value at infinite separation.  $\psi_s(\theta; x)$  is calculated using the full nonlinear PB equation that includes details of the number density of ionizable groups,  $\Gamma$ , salt concentration,  $c_0$ , pH, and pK. We emphasize that the purpose of the approximation in eq 7 is to offer simple mechanistic insight into the physical trends underlying the behavior. It is accurate in a situation where  $\Delta \psi_s(\theta; x) \ll 1$ , implying that  $\psi_s(\theta; x)$  is only weakly perturbed by the approach of another object. Because of the exponential nature of the screening of the electrical potential, this condition is generally met at long range ( $x \gtrsim 2\kappa^{-1}$ ), the region of interest in our problem. At shorter range, the quality of the approximation is likely to be poorer, and in this case, eq 6 will have to be used. As indicated by eq 4, the total interfacial energy at separation  $x$  is then given by

$$\begin{aligned} \Delta F_{\text{int}} &= 2\pi R^2 \int_0^\pi \Delta f_{\text{int}}(\theta; x) \sin \theta d\theta \\ &\approx 2\pi R^2 z e \varphi_{\text{int}}(\psi_{s, \infty}) \Gamma \frac{d\alpha}{d\psi} \Big|_{\psi_{s, \infty}} \times \int_0^\pi \Delta \psi_s(\theta; x) \sin \theta d\theta \end{aligned} \quad (9)$$

Importantly, the separation dependence of  $\Delta F_{\text{int}}$  reflects that of the integral of  $\Delta \psi_s(\theta; x)$  over the sphere surface. We will show in subsequent sections that

$$I_{\text{int}} = \int_0^\pi \Delta \psi_s(\theta; x) \sin \theta d\theta = C_1 \psi_{s, \infty} \exp(-\kappa_{\text{int}} x) \quad (10)$$

where in the regime  $\kappa R \gg 1$ , we have  $C_1 \approx 1/2\kappa R$ , which is approximately known from the analysis in the linear PB regime discussed in the following section. We point out that the approximation in eq 9 is accurate in the regime of low surface charge density, which, in turn, correlates with small surface potentials, that is,  $|\psi_{s, \infty}| \ll 1$ . Combining eqs 9 and 10, we may write, in general

$$\Delta F_{\text{int}} = B \exp(-\kappa_{\text{int}} x) \quad (11)$$

where  $\kappa_{\text{int}}$  is the effective inverse decay length of the interfacial free energy,  $\Delta F_{\text{int}}$ , and

$$B \approx 2\pi R^2 C_1 \epsilon z \varphi_{\text{int}}(\psi_{s,\infty}) \Gamma \frac{d\alpha}{d\psi} \bigg|_{\psi_{s,\infty}} \psi_{s,\infty} \quad (12)$$

is a coefficient that ultimately determines the sign and magnitude of the interfacial contribution. Importantly,  $\kappa_{\text{int}} \neq \kappa$ ; in fact, we will show later that, in general,  $\kappa_{\text{int}} < \kappa$ . When  $B < 0$ , the sign of  $\Delta F_{\text{int}}$  is negative, implying that the interfacial contribution generates an attractive interaction between the two particles.

Furthermore, for small values of charge density, given by  $|\sigma| < 0.01e/\text{nm}^2$ , typical of most experiments, we can further simplify eq 12 by setting  $\varphi_{\text{int}} \approx \varphi_0$ . Our molecular simulation studies provide an estimate of  $\varphi_0 \approx -0.3\text{ V} < 0$  for water. Importantly, eq 12 points to the following trends. For negatively charged particles in water, we have  $\psi_{s,\infty} < 0$ . Provided that  $d\alpha/d\psi \neq 0$ , our model suggests that in water: (1)  $B < 0$  for negatively charged particles when  $\sigma$  is small (as  $\varphi_{\text{int}} < 0$  for  $|\sigma| < 0.3e/\text{nm}^2$ ); (2)  $B > 0$  for negative particles when  $|\sigma| \gtrsim 0.3e/\text{nm}^2$ , as here  $\varphi_{\text{int}} > 0$ ; and (3)  $B > 0$  for positive particles, regardless of the magnitude of  $\sigma$ , because here  $\psi_{s,\infty} > 0$  and  $\varphi_{\text{int}} < 0$  (Figure 1). Because surfaces in solution rarely exceed a charge density of  $|\sigma| \approx 0.3e/\text{nm}^2$ , eq 12 implies that in water, the interfacial contribution generates an attractive force between negatively charged particles, a repulsive force for positively charged particles, and vice versa for a solvent where  $\varphi_0 > 0$ . Equation 12 also suggests that the interfacial contribution to the total interaction is maximal when  $|z d\alpha/d\psi|$  is maximal and should vanish when  $d\alpha/d\psi \rightarrow 0$ . Ref 31 provides a map of various conditions involving the pH, pK, salt concentration,  $c$ , and group density,  $\Gamma$ , under which the interfacial attraction is likely to manifest in experiment.

Note that for particles carrying a mixture of acidic and basic groups such as proteins, interesting trends may emerge for the sign of the interfacial term,  $\Delta F_{\text{int}}$ . We consider for a moment the interaction of weakly charged objects carrying a mixture of acidic and basic groups, where the sign of net charge on the particles (reflected in  $\psi_{s,\infty}$ ) is dominated by either the positive or negative ionized groups. Despite the qualitatively different responses of the net charge of the two types of groups to interparticle separation, we may still expect the sign of the interfacial free energy, given by that of  $B$ , to remain the same as that in a situation where the particles carry a single species of charged groups of the same sign as the dominant species in the case of mixed groups. This is because both  $z$  and  $d\alpha/d\psi$  are of different signs for the acidic and basic species, which gives the same overall sign of  $B$  for each type of group individually. The present study, however, focuses on the simplest of systems where the objects carry ionizable groups of the same qualitative nature, either acidic or basic.

Finally, we point out that in the present analysis, the dielectric interior of the interacting particles has been excluded from the computation of electrostatic interaction free energies,  $\Delta F_{\text{el}}$ . For spheres at infinite separation carrying uniform surface charge, the electrical potential inside each sphere is uniform, and the electric field,  $\mathbf{E}$ , inside the sphere is zero everywhere. Therefore, the self-energy contribution from the spheres' interior, whose dielectric constant is  $\epsilon_s$ , is given by the integral  $1/2 \int_V \epsilon_s \epsilon_0 \mathbf{E}^2 dV$  over the spheres' volume and is also zero. As two spheres approach each other, however, the symmetry in  $\theta$  is broken, and  $\mathbf{E}$  becomes nonzero in the spheres' interior in the region of closest approach. This should give a net positive contribution to the total free energy. Calculating this quantity, we find that the typical magnitude of the interior contribution is on the order of  $10^{-6}$  of the total free energy, which is negligible. The inclusion of a dielectric interior in the solution of the PB equation with eq 2 as the boundary condition has an additional minor effect: It alters the surface potential of the sphere,  $\psi_s(\mathbf{R})$ , and therefore the value of  $\alpha(\mathbf{R})$  slightly. There is a small quantitative change in  $\Delta F_{\text{int}}$  that therefore also slightly alters the depth of the minimum in the interparticle potential. However, we have ignored these small contributions for the purpose of illustrating broad qualitative trends that remain unaffected by the detailed properties of the sphere interior. Similarly, our present analysis also excludes the Stern layer, which is typically modeled as a thin, low-dielectric, charge-free region at the particle surface.<sup>64</sup> The inclusion of such detail is likely to result in a small shift of the fitted value of  $p$  when modeling the experimental measurements.

### 3. RESULTS AND DISCUSSION

**3.1. Comparing the Distance Dependence of the Interfacial and Electrostatic Free Energies in the Linear and Nonlinear PB Regimes.** We begin by considering the interparticle separation dependence of the interfacial and electrostatic free-energy terms in the linear PB regime ( $|\eta\rangle \ll 1$ ). The spatial potential distribution in a system consisting of two approaching spherical particles is given by the solution of the Debye–Hückel equation

$$\nabla^2 \psi = \kappa^2 \psi \quad (13)$$

subject to appropriate boundary conditions at the surface of the particles ( $\psi = \psi_s$ ) and at infinity ( $\psi = 0$ ). The analytical solution to this equation for two identical spheres is described by an infinite series.<sup>65,66</sup> However, it can be shown that for large interparticle distances,  $x$ , the potential field can be well-approximated by superposition of the potentials of two isolated spheres.<sup>67,68</sup> The solution to eq 13 for a single sphere of radius  $R$  is given by<sup>69</sup>

$$\psi = \psi_{s,\infty} \frac{R}{\rho} \exp\left[-\kappa R \left(\frac{\rho}{R} - 1\right)\right] \quad (14)$$

which is valid for all values of  $\kappa R$  provided that the surface potential of the isolated sphere is  $|\psi_{s,\infty}| \ll 1$ . Here  $\rho$  represents the distance of a point from the center of the particle.

Accordingly, for two identical particles separated by a distance  $x$ , the potential  $\psi$  at any point  $S$  is approximated by

$$\psi(\rho_1, \rho_2) = \psi_{s,\infty} \frac{R}{\rho_1} \exp\left[-\kappa R \left(\frac{\rho_1}{R} - 1\right)\right] + \psi_{s,\infty} \frac{R}{\rho_2} \exp\left[-\kappa R \left(\frac{\rho_2}{R} - 1\right)\right] \quad (15)$$

where  $\rho_1$  and  $\rho_2$  are the distances between point  $S$  and the centers of the spheres (Figure 3). The above equation implies

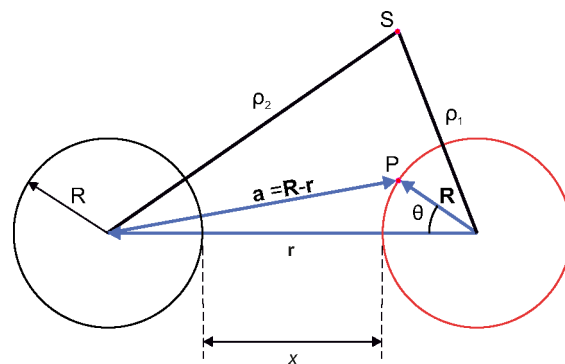


**Figure 3.** Two charged particles approaching one another. For large separations,  $x$ , the potential at a point  $S$  can be approximated by superposition of the potentials of two isolated spheres.

that the potential difference,  $\Delta\psi_s$ , at any point  $P$  on the surface of either sphere is given by

$$\Delta\psi_s(\theta; x) = \psi_{s,\infty} \frac{R}{a} \exp\left[-\kappa R \left(\frac{a}{R} - 1\right)\right] \quad (16)$$

which is simply the potential due to the approaching particle evaluated at the surface contour of the sphere of interest (Figure 3). Here  $a$  and  $R$  are magnitudes of vectors  $\mathbf{a}$  and  $\mathbf{R}$ , respectively,

and  $\psi_{s,\infty}$  is the surface potential of the charged particles as  $x \rightarrow \infty$ . Noting that  $|r| = r = x + 2R$  and  $\mathbf{a} = \mathbf{R} - \mathbf{r}$ , we can write

$$\Delta\psi_s(\theta; x) = \frac{\psi_{s,\infty} \exp(\kappa R)}{h(\theta; x)} \exp[-\kappa R h(\theta; x)] \quad (17)$$

where

$$h(\theta; x) = \left[ 5 + \left(\frac{x}{R}\right)^2 + 4\left(\frac{x}{R}\right) - 2\left[\left(\frac{x}{R}\right) + 2\right] \cos \theta \right]^{1/2}$$

The integral of interest in eq 10 is then given by

$$I_{\text{int}} = \int_0^\pi \Delta\psi_s(\theta; x) \sin \theta d\theta = \psi_{s,\infty} C_2 \left[ \frac{\exp(-\kappa x)}{x/R + 2} \right] \quad (18)$$

where  $C_2 = (1 - \exp(-2\kappa R))/\kappa R$ . Combining eq 18 with eq 6 gives, in the regime of low surface potentials ( $|\psi_s| \ll 1$ )

$$\Delta F_{\text{int}} \propto \left[ \frac{\exp(-\kappa x)}{x/R + 2} \right] \quad (19)$$

The electrostatic interaction free-energy,  $\Delta F_{\text{el}}$ , for two spherical charged particles, in turn, can be approximated by<sup>67,69</sup>

$$\frac{\Delta F_{\text{el}}}{k_B T} = C_3 \left( \frac{R}{l_B} \right) \left[ \frac{\exp(-\kappa x)}{x/R + 2} \right] \quad (20)$$

where  $l_B = e^2/4\pi\epsilon_0\epsilon_r k_B T$  is the Bjerrum length. Here  $C_3 = \psi_{s,\infty}$  for spheres at constant potential, and  $C_3 = 4\pi\sigma l_B R/[e(1 + \kappa R)]$  for spheres of constant surface charge density,  $\sigma$ . The above expression is valid for small surface potentials ( $|\psi_s| \ll 1$ ) and all  $\kappa R$  values if  $\kappa x$  is sufficiently large. The above two equations indicate that in the linear regime, the distance dependences of both  $\Delta F_{\text{int}}$  and  $\Delta F_{\text{el}}$  are described by the same functional form. In other words, the ratio  $\Delta F_{\text{int}}/\Delta F_{\text{el}}$  is independent of  $x$ .

We now compare the numerically evaluated electrostatic free energy,  $\Delta F_{\text{el}}$ , and the interfacial hydration contribution,  $\Delta F_{\text{int}}$ , with the corresponding approximations in the linear regime given by eqs 20 and 19, respectively. We numerically solve the NLPB equation for spheres of radius  $3.25 \mu\text{m}$  immersed in an electrolyte where  $\kappa^{-1} = 235 \text{ nm}$ . We consider two different values of constant surface charge such that  $|\psi_{s,\infty}| \approx 0.2$  and  $5k_B T$ , representing the linear and nonlinear regimes, respectively. In the regime of low surface potentials,  $|\psi_s| \ll 1$ , we expect the analytical results of eqs 20 and 19 to accurately capture the numerically calculated results. To compare calculated results with the corresponding analytical expressions, we examine the distance dependence of the ratios  $\Delta F_{\text{el}}/\Delta F_{\text{el}}^{\text{SC}}$  and  $\Delta F_{\text{int}}/\Delta F_{\text{int}}^{\text{SC}}$ , where the superscript SC denotes a screened Coulombic functional form, as given in eqs 20 and 19. We omit any pre-exponential factors as we are interested in comparing the forms of the spatial decay rather than exact magnitudes. We therefore normalize the ratios to their values at  $\kappa x > 2$  to facilitate comparison. For low values of  $|\psi_s|$ , the expression for  $\Delta F_{\text{el}}$  based on the linearized PB equation is expected to hold. Figure 4a confirms this expectation and shows that for  $\kappa x > 2$ , the screened Coulombic functional form indeed provides an accurate distance dependence of both  $\Delta F_{\text{el}}$  and  $\Delta F_{\text{int}}$ . However, at short range,  $\kappa x < 2$ , we note that the magnitude of  $\psi_s$  progressively increases, implying a transition from the linear to the nonlinear regime. This transition out of the linear regime at small separations is reflected in the calculated separation dependence

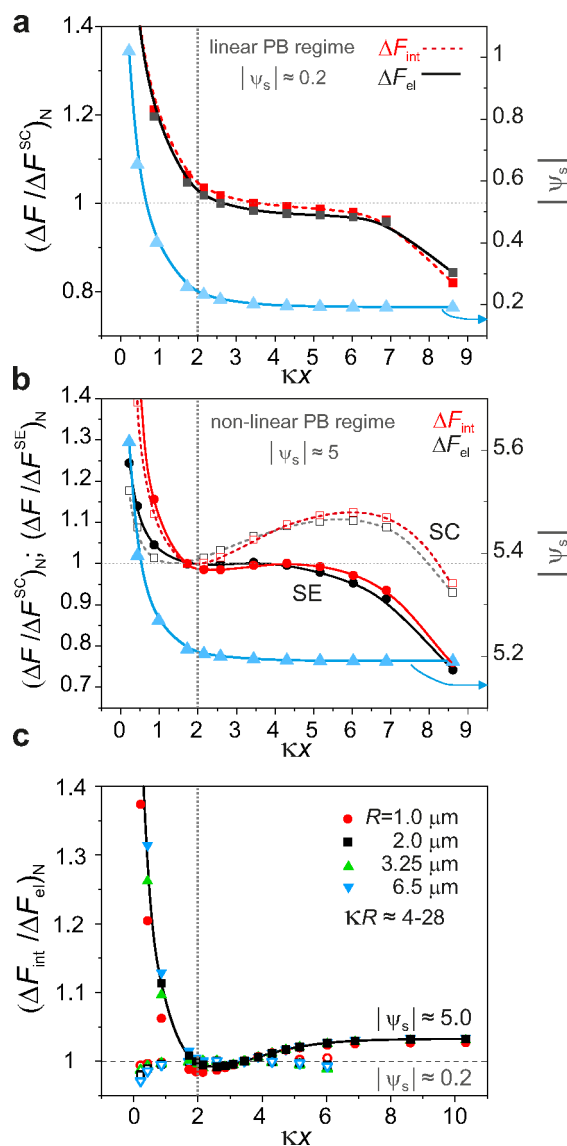


**Figure 4.** Comparing the calculated distance dependence of  $\Delta F_{\text{el}}$  and  $\Delta F_{\text{int}}$  with the screened Coulombic,  $\Delta F^{\text{SC}}$ , and simple exponential,  $\Delta F^{\text{SE}}$ , functional forms in both the linear and nonlinear PB regimes.  $c_0 = 1.66 \mu\text{M}$  in all cases, which corresponds to  $\kappa^{-1} = 235 \text{ nm}$ . (a) Plots of the ratios  $(\Delta F_{\text{el}}/\Delta F^{\text{SC}})_N$  (black solid line and symbols) and  $(\Delta F_{\text{int}}/\Delta F^{\text{SC}})_N$  (red dashed line and symbols) obtained by solving the NLPB equation (eq 1) for particles of radius  $R = 3.25 \mu\text{m}$  interacting at constant charge,  $\sigma = -10^{-4} e/\text{nm}^2$  ( $\Gamma = 10^{-4}/\text{nm}^2$ ,  $p = -10$  in eqs 2 and 3), in the regime of low surface potentials, where  $|\psi_{s,\infty}| \approx 0.2$  (blue triangles). Ratios are normalized such that their values at  $\kappa x \approx 3$  are unity in all cases. (b) Plots of various ratios in the nonlinear regime corresponding to  $|\psi_{s,\infty}| \approx 5$ , calculated using charge regulation boundary conditions where  $p = -2.2$  and  $\Gamma = 0.014/\text{nm}^2$ :  $(\Delta F_{\text{el}}/\Delta F^{\text{SC}})_N$  (black squares, dashed line),  $(\Delta F_{\text{int}}/\Delta F^{\text{SC}})_N$  (red squares, dashed line),  $(\Delta F_{\text{el}}/\Delta F^{\text{SE}})_N$  (black circles, solid line), and  $(\Delta F_{\text{int}}/\Delta F^{\text{SE}})_N$  (red circles, solid line). (c) Plot of  $(\Delta F_{\text{int}}/\Delta F_{\text{el}})_N$  in the linear (open symbols) and nonlinear (filled symbols) regimes, calculated as described in panels a and b, respectively, for particle radii  $R = 1$  (red circles),  $2$  (black squares),  $3.2$  (green triangles), and  $6.5 \mu\text{m}$  (blue inverted triangles). All lines are visual guides.

of the two quantities, both of which depart strongly from those of the analytical approximations.

Next we compare the calculated values of  $\Delta F_{\text{el}}$  and  $\Delta F_{\text{int}}$  in the regime of large  $|\psi_s|$  with both the screened Coulombic (SC) and the simple exponential (SE), functional forms. We find that neither the SC form, that is,  $\Delta F^{\text{SC}} \propto \exp(-\kappa r)/r$ , nor the simple exponential,  $\Delta F^{\text{SE}} \propto \exp(-\kappa x)$ , perfectly captures the distance dependence of  $F_{\text{el}}$  over the entire range of separations  $x$  (Figure 4b). Interestingly, we note that in the range of interest,  $\kappa x > 2$ , the simple exponential in fact provides the better description of the calculated data (solid circles, Figure 4b). This further justifies our assumption that under the conditions of  $\kappa x$  and  $\kappa R$  of interest, the electrostatic free energy can indeed be described by a single exponential at long range, such that  $\Delta F_{\text{el}} \propto \exp(-\kappa_1 x)$ , where the screening length  $\kappa_1 \approx \kappa$ . Yet again at short range  $\kappa x < 2$ , we note strong departures of both  $\Delta F_{\text{el}}$  and  $\Delta F_{\text{int}}$  from both the screened Coulombic and simple exponential forms.

Having examined in detail the distance dependence of both the electrostatic free energy and the interfacial free energy, we next examine the ratio  $\Delta F_{\text{int}}/\Delta F_{\text{el}}$  as a function of separation,  $\kappa x$ , for a range of particle radii,  $R = 1$  to  $6.5 \mu\text{m}$  and  $\kappa^{-1} = 235 \text{ nm}$ . To facilitate comparison, we consider the quantity  $(\Delta F_{\text{int}}/\Delta F_{\text{el}})_N$ , which is the ratio of free-energy contributions in each case normalized to its value at the separation  $\kappa x = 3.4$  (Figure 4c). For  $|\psi_s| \approx 0.2$ , the system is in the linear regime, and we find that  $(\Delta F_{\text{int}}/\Delta F_{\text{el}})_N$  is constant over the range of  $\kappa x$  of interest, as expected (open symbols, Figure 4c). However, for  $|\psi_s| \approx 5$ , we note that at long range,  $\kappa x > 2$ , the ratio  $(\Delta F_{\text{int}}/\Delta F_{\text{el}})_N$  increases with respect to distance. Importantly, this indicates a more gradual spatial decay of the interfacial free-energy term,  $\Delta F_{\text{int}}$ , relative to its repulsive, electrostatic free-energy counterpart,  $\Delta F_{\text{el}}$ .

We then examine the influence of ionic strength on the spatial behavior of the ratio  $(\Delta F_{\text{int}}/\Delta F_{\text{el}})_N$ . We repeat the analysis for large spheres of radii  $R = 1$  to  $6.5 \mu\text{m}$ , decreasing the Debye lengths from  $\kappa^{-1} \approx 235$  to  $\sim 8 \text{ nm}$ . We note that for a given Debye length, the functional form of the quantity  $(\Delta F_{\text{int}}/\Delta F_{\text{el}})_N$  remains remarkably similar over a range of  $R$  as long as  $\kappa R$  is large (Figure 5a), but we note that for very large  $\kappa R$ , achieved by reducing  $\kappa^{-1}$ , the functional form of the ratio changes significantly. The range of separation over which the ratio increases monotonically shifts systematically to smaller values of  $\kappa x$ , as shown in Figure 5a.

Finally, we examine the opposite limit of the point object, that is,  $\kappa R \ll 1$ . We find that in general, in the limit of very small spheres, the nonmonotonic behavior largely vanishes, that is,  $(\Delta F_{\text{int}}/\Delta F_{\text{el}})_N \approx 1$ , over the entire range of  $\kappa x$  (Figure 5b). In general, this suggests a total interaction potential displaying only monotonic behavior, either attractive or repulsive, as discussed further in the following section. However, we find that even within the nonlinear PB regime, characterized by  $|\psi_s| \gtrsim 1$ , the distance dependence of the ratio  $(\Delta F_{\text{int}}/\Delta F_{\text{el}})_N$  proves to be highly dependent on the particular value of  $\psi_s$  for a given  $\kappa R$  (compare closed and open triangular and square symbols, Figure 5b). The sensitivity of the problem to an additional property of the particle, namely, its surface charge, renders the extraction of a simple geometry-related trend governing the distance dependence of  $(\Delta F_{\text{int}}/\Delta F_{\text{el}})_N$  challenging.

**3.2. Nonmonotonic Total Free Energy in the Nonlinear PB Regime.** In this section, we consider the interparticle interaction at large separations,  $\kappa x > 2$ . We will show that a more gradual decay of  $\Delta F_{\text{int}}$  compared with  $\Delta F_{\text{el}}$  can result in a long-

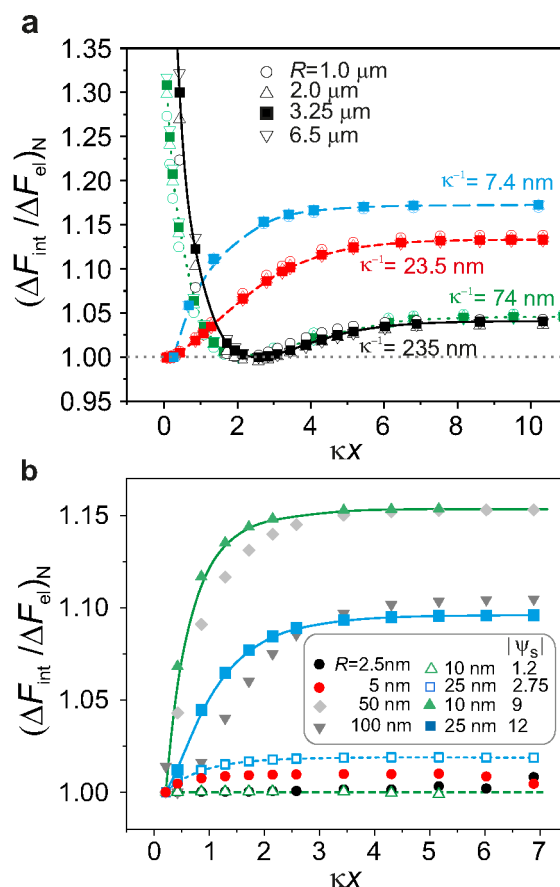


**Figure 5.** (a) Spatial dependence of the ratio  $(\Delta F_{\text{int}}/\Delta F_{\text{el}})_N$  on the Debye length,  $\kappa^{-1}$ , for various particle radii,  $R$ , in the large  $\kappa R$  regime such that  $\kappa R \approx 4$ – $900$ . We use constant charge boundary conditions with  $\sigma = -0.14e/\text{nm}^2$  ( $\Gamma = 0.14/\text{nm}^2$ ,  $p = -10$ ), except where specified, which generally yields  $|\psi_{s,\infty}| \gtrsim 3$ . We consider particle radii  $R = 1$  (open circles),  $2$  (upright triangles),  $3.25$  (squares), and  $6.5 \mu\text{m}$  (inverted triangles) and Debye lengths  $\kappa^{-1} = 7.4$  (blue long-dashed lines),  $23.5$  (red dashed lines),  $74$  (green dotted lines), and  $235 \text{ nm}$  (black solid lines). (b) Spatial dependence of the ratio  $(\Delta F_{\text{int}}/\Delta F_{\text{el}})_N$  on the particle radius in the small  $\kappa R$  regime,  $\kappa R \approx 0.01$ – $0.4$  where  $\kappa^{-1} = 235 \text{ nm}$  and particle radius  $R = 2.5$  (black circles),  $5$  (red circles),  $10$  (upright triangles),  $25$  (squares),  $50$  (diamonds), and  $100 \text{ nm}$  (inverted triangles). Open and filled symbols for  $R = 10$  (triangles) and  $25 \text{ nm}$  (squares) denote low and high values of surface potential in the regime  $|\psi_s| > 1$ , respectively. Here we consider lower values of  $|\psi_{s,\infty}| = 1.2$  and  $2.75$  (corresponding to  $\sigma = -0.014e/\text{nm}^2$ ) and higher values of  $|\psi_{s,\infty}| = 9$  and  $12$  (corresponding to  $\sigma = -0.14e/\text{nm}^2$ ). All lines are visual guides.

range minimum in the total interaction free energy,  $\Delta F_{\text{tot}}$ . To illustrate this, we rewrite  $\Delta F_{\text{tot}}$  as follows

$$\begin{aligned} \Delta F_{\text{tot}} &= \left( 1 + \frac{\Delta F_{\text{int}}}{\Delta F_{\text{el}}} \right) \Delta F_{\text{el}} \\ &\approx A \left( 1 - \frac{|\Delta F_{\text{int}}|}{\Delta F_{\text{el}}} \right) \exp(-\kappa_1 x) = A \Delta F'_{\text{tot}} \end{aligned} \quad (21)$$

where  $\Delta F_{\text{int}} = -|\Delta F_{\text{int}}|$  explicitly accounts for the negative sign of the  $\Delta F_{\text{int}}$  interfacial contribution term in the interaction of negatively charged particles in water. The negative sign is here crucial to the appearance of the long-range minimum in the net pair potential because otherwise, the two contributions simply reinforce each other, and a minimum cannot arise. Figure 6a

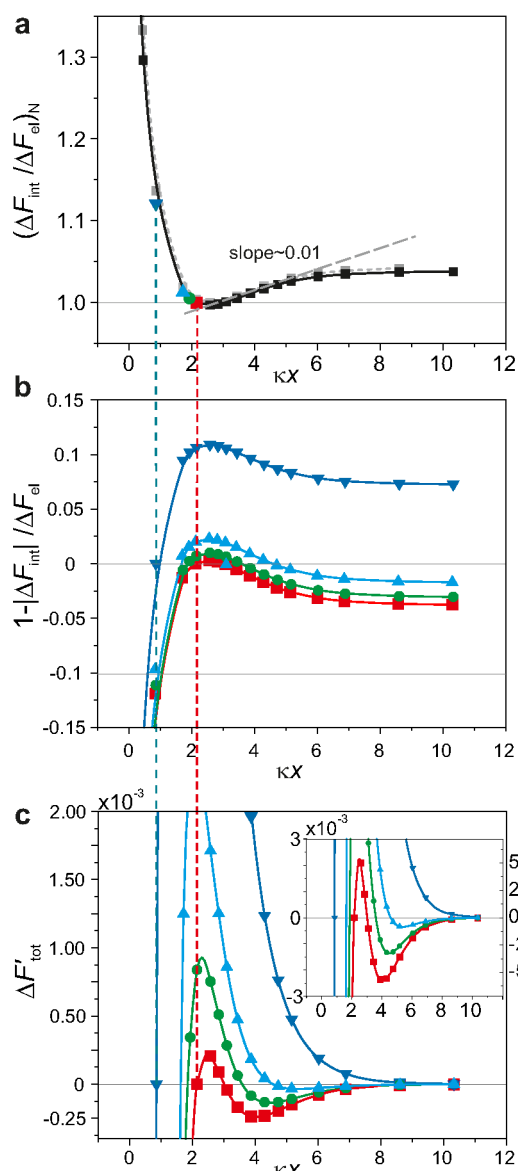


**Figure 6.** Graphical depiction of the appearance of nonmonotonic interaction potentials,  $\Delta F_{\text{tot}}$  from a nonmonotonic  $(|\Delta F_{\text{int}}|/\Delta F_{\text{el}})_N$  function. (a)  $(|\Delta F_{\text{int}}|/\Delta F_{\text{el}})_N$  for charge regulation ( $\Gamma = 0.014/\text{nm}^2$ ,  $p = -2.2$ , solid line) and constant charge boundary conditions ( $\Gamma = 0.01/\text{nm}^2$ ,  $p = -10$  dashed line) normalized to their respective minimum values over the entire range of  $\kappa x$ . Here  $R = 3.25 \mu\text{m}$  and  $\kappa^{-1} = 235 \text{ nm}$ , as in the experiment considered in Figure 2. (b) Spatial dependence of the function  $1 - |\Delta F_{\text{int}}|/\Delta F_{\text{el}}$  generated by normalizing  $|\Delta F_{\text{int}}|/\Delta F_{\text{el}}$  to its value at  $\kappa x^* = 0.9$  (dark blue inverted triangles), 1.7 (blue triangles), 1.9 (green circles), and 2.15 (red squares). (c) Spatial dependence of the dimensionless interaction potential  $\Delta F'_{\text{tot}} = (1 - |\Delta F_{\text{int}}|/\Delta F_{\text{el}}) \exp(-\kappa x)$  for the four  $\kappa x^*$  values. The inset depicts the possibility of well depths  $|w| \approx 0.1 - 5k_B T$  at locations  $\kappa x_{\text{min}} \approx 4-6$  under the conditions considered. All lines are visual guides.

displays the calculated value of the ratio  $(|\Delta F_{\text{int}}|/\Delta F_{\text{el}})_N$  as a function of separation, which is nothing but the ratio  $|\Delta F_{\text{int}}|/\Delta F_{\text{el}}$  normalized to its minimum value over the entire range of separations. If  $(|\Delta F_{\text{int}}|/\Delta F_{\text{el}})_N = 0$  or constant over the entire distance range, then eq 21 implies a total interaction potential,  $\Delta F_{\text{tot}}$  that has the monotonic character of  $\exp(-\kappa x)$ . However, Figures 5–7a illustrate that in general,  $(|\Delta F_{\text{int}}|/\Delta F_{\text{el}})_N$  is not constant with respect to  $x$ . We remark here that the nature of the

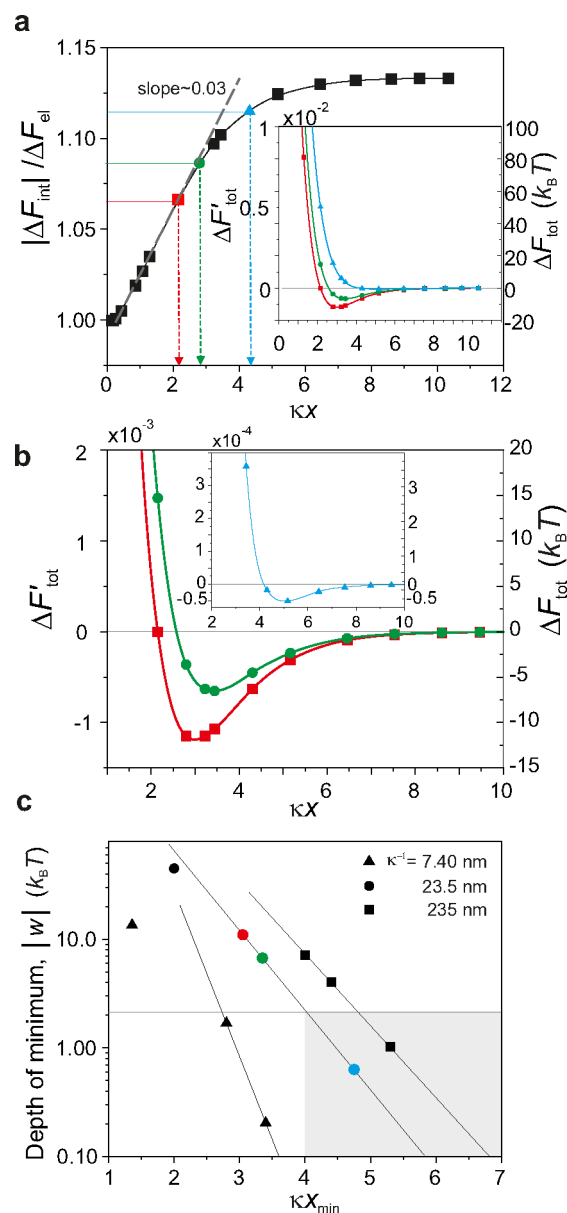


**Figure 7.** (a)  $(|\Delta F_{\text{int}}|/\Delta F_{\text{el}})_N$  calculated for particles of radius  $R = 3.25 \mu\text{m}$  using  $\kappa^{-1} = 235 \text{ nm}$  and charge regulation boundary conditions ( $\Gamma = 0.014/\text{nm}^2$ ,  $p = -2.2$ , solid line).  $\Delta F'_{\text{tot}}$  and  $\Delta F_{\text{tot}}$  corresponding to three values of  $\kappa x^* = 2.15$  (red squares), 2.8 (green circles), and 4.3 (blue triangles) (inset). (b) View of pair potentials around the region of the minima that indicate the possibility of well depths  $|w| \approx 0.1 - 5k_B T$  at locations  $\kappa x_{\text{min}} \approx 4-6$  under the conditions considered. (c) Plot of expected well depth magnitudes,  $|w|$ , as a function of their location  $\kappa x_{\text{min}}$  for three values of salt concentration corresponding to  $\kappa^{-1} = 7.4$  (triangles), 23 (circles), and 235 nm (squares). Minima of depth  $|w| \approx 1k_B T$  could be expected to occur at  $\kappa x_{\text{min}} \approx 4-7$  (shaded) for  $\kappa^{-1} \gtrsim 20 \text{ nm}$ . All lines are visual guides.

boundary condition, whether constant charge or charge regulation, makes little qualitative difference to the separation dependence of  $(|\Delta F_{\text{int}}|/\Delta F_{\text{el}})_N$  (Figure 6a). Regardless, we perform all analyses using charge regulation boundary conditions to remain as close to the experimental situation as possible.

When  $B < 0$ , we have  $\Delta F_{\text{int}}(x) < 0$  everywhere, and the form of the nonmonotonic spatial behavior of  $(|\Delta F_{\text{int}}|/\Delta F_{\text{el}})_N$  suggests the possibility of alternating minima and maxima in  $\Delta F_{\text{tot}}$ . To

illustrate this point, we generate various pair potentials, setting  $|\Delta F_{\text{int}}|/\Delta F_{\text{el}} = 1$  at four different values of interparticle separation,  $x$ , denoted by  $x^*$  (Figure 6). The assumption here is that the magnitudes of the two free-energy contributions, that is,  $|\Delta F_{\text{int}}|$  and  $\Delta F_{\text{el}}$ , are equal at a particular value of  $x = x^*$ . The qualitative origin of the minimum in  $\Delta F_{\text{tot}}$  is already evident in the spatial variation of the quantity  $1 - |\Delta F_{\text{int}}|/\Delta F_{\text{el}}$  (Figure 6b). We note that the location,  $x_{\text{min}}$ , and the depth of the minimum,  $w$ , both depend on the value of  $x^*$ . Figure 6 illustrates the principle graphically for various values of  $\kappa x^*$  for particles of radius  $R = 3.25 \mu\text{m}$  and  $\kappa^{-1} \approx 235 \text{ nm}$  radius. Figure 4c further shows that the same qualitative behavior may be generally expected for large spheres corresponding to the regime of large  $\kappa R > 4$ . For any given  $\Delta F'_{\text{tot}}$  profile, the value of the interaction energy given by  $\Delta F_{\text{tot}}$  may be deduced from the value of  $A$ , which can, in turn, be estimated either from an exponential fit to the full nonlinear calculation of  $\Delta F_{\text{el}}$ , as shown in Figure 2b, or very crudely from the LPB approximation, eq 20. In the case illustrated for  $R = 3.25 \mu\text{m}$ ,  $c = 1.66 \mu\text{M}$ , and  $\sigma = -0.014\text{e/nm}^2$ , corresponding to  $\kappa R \approx 14$ , we find that  $A \approx 2.4 \times 10^4 k_{\text{B}}T$ . This implies minima of depth  $w \approx 1 - 6k_{\text{B}}T$  occurring at separations of  $4 - 6\kappa^{-1}$ . We further find that under these conditions, long-range minima in the pair potential are associated with energy barriers of height  $10 - 60k_{\text{B}}T$  (Figure 6c). Thus, in general, we find that this model supports the occurrence of stable pair-potential minima of depths of  $1 - 5k_{\text{B}}T$  at separations in the range  $x_{\text{min}} \gtrsim 5\kappa^{-1}$ , in particular, in the regime of low ionic strengths,  $c_0 = 1 - 10 \mu\text{M}$ , as observed in experiment. We find that the disparity in the separation dependent decay of the repulsion and attraction terms is responsible for the appearance of stable pair-potential minima within our model.

Repeating the analysis for  $R = 3.25 \mu\text{m}$  and higher salt concentration, up to  $c_0 \approx 1.6 \text{ mM}$ , we note a progressive shift of the pair-potential minima to smaller separation and therefore a reduction in  $\kappa x_{\text{min}}$  (Figure 7a,b). For  $c_0 \approx 160 \mu\text{M}$ , for instance, we find that a minimum of depth  $|w|$  in the pair potential is expected to occur at progressively smaller values of  $\kappa x_{\text{min}}$  compared with at  $c_0 \approx 1.6 \mu\text{M}$  (Figure 7c). We further note a systematic reduction in the depth of the minimum,  $|w|$ , with increasing  $\kappa x_{\text{min}}$  at all salt concentrations. Thus any minima occurring at large interparticle separations corresponding to ( $\kappa x_{\text{min}} > 5$ ) are expected to get shallower ( $|w| \ll 5k_{\text{B}}T$ ) with increasing salt concentration (shaded region, Figure 7c). In general, we find that particle properties remaining constant, increasing the ionic strength reduces the depth of a possible long-range minimum at a given separation (Figure 7c). This trend would be expected solely on account of the fact that  $\Delta F_{\text{tot}} \propto A \propto \psi_s^2$ , and the surface potential  $\psi_s \propto \kappa \propto c_0^{-1/2}$  decreases with increasing salt concentration. It is worth noting, however, that in practice, the dependence of the long-range minimum on salt concentration is likely to be more strongly determined by other factors such as  $d\alpha/d\psi$ , which controls the magnitude of  $B$ . For example, when  $|p|$  is large,  $d\alpha/d\psi \rightarrow 0$ , implying  $B \rightarrow 0$ . In particular when  $p < 0$ , which generally holds for acidic surface groups, an increase in salt concentration decreases the magnitude of  $\psi_s$  and consequently that of  $B$ .  $B \rightarrow 0$  renders the condition  $|\Delta F_{\text{int}}| = \Delta F_{\text{el}}$  impossible to meet, except at  $\kappa x \rightarrow \infty$ , where both quantities go to zero. Thus under these conditions, the long-range minimum is expected to vanish, and the pair potential follows the monotonic DLVO prediction.

Finally, we note that in the range of separation of interest ( $\kappa x \gtrsim 2$ ), the ratio  $(|\Delta F_{\text{int}}|/\Delta F_{\text{el}})_N$  may be approximated by a linear function (Figures 6a and 7a). Thus we write

$$\begin{aligned} |\Delta F_{\text{int}}| &\propto (1 + m\kappa x)\Delta F_{\text{el}} \\ &\propto \exp(m\kappa x) \exp(-\kappa_{\text{el}}x) \\ &\propto \exp(-\kappa_{\text{int}}x) \end{aligned} \quad (22)$$

where the slope  $m \approx 0.01 - 0.05$  for the conditions considered. This implies that in general, for large colloidal spheres at low ionic strengths,  $\kappa_{\text{el}}/\kappa_{\text{int}} \approx 1.01 - 1.05$ .

### 3.3. Location of the Minimum in the Pair Potential.

Having explored the origin of the two different screening lengths for each term in eq 5, we now consider the implications thereof for the location of the spatial minimum in the pair-interaction energy. For a pair potential of the form given by eq 5, with parameters  $A > 0$  and  $B < 0$  and screening lengths  $\kappa_{\text{el}} > \kappa_{\text{int}}$ , a minimum occurs at an intersurface separation given by

$$x_{\text{min}} = \frac{\kappa_{\text{el}}^{-1}\kappa_{\text{int}}^{-1}}{\kappa_{\text{int}}^{-1} - \kappa_{\text{el}}^{-1}} \ln\left(-\frac{A\kappa_{\text{int}}^{-1}}{B\kappa_{\text{el}}^{-1}}\right) \quad (23)$$

Because by definition, the quantity  $-A\kappa_{\text{int}}^{-1}/B\kappa_{\text{el}}^{-1} > 1$  and, in general,  $\kappa_{\text{el}} \approx \kappa_{\text{int}} \approx \kappa$ , we may write

$$\kappa x_{\text{min}} \approx \left(\frac{\kappa_{\text{el}}}{\kappa_{\text{int}}} - 1\right)^{-1} \ln\left(-\frac{A}{B}\right) \quad (24)$$

For the general case where  $A$  is only slightly larger than  $|B|$  so that  $A/|B| = 1 + s$ , where  $s \ll 1$ , we expect  $\kappa x_{\text{min}} \approx s(\kappa_{\text{el}}/\kappa_{\text{int}} - 1)^{-1} = 20s - 100s$ .

Knowing from measurement the location of the minimum in the pair potential,  $x_{\text{min}}$ , and the value of the interaction free energy at the minimum,  $\Delta F(x_{\text{min}}) = w < 0$  (Figure 2b), using eqs 5 and 23, we have

$$A = -\frac{w\kappa_{\text{int}} \exp(\kappa_{\text{el}}x_{\text{min}})}{\kappa_{\text{el}} - \kappa_{\text{int}}} \quad (25)$$

$$B = \frac{w\kappa_{\text{el}} \exp(\kappa_{\text{int}}x_{\text{min}})}{\kappa_{\text{el}} - \kappa_{\text{int}}} \quad (26)$$

and

$$\left|\frac{A}{B}\right| \approx 1 + m\kappa x_{\text{min}} + (m\kappa x_{\text{min}})^2 \quad (27)$$

The above expressions could guide fits of experimental data to eq 5, where  $x_{\text{min}}$  and  $w$  are measured, provided system parameters such as  $\kappa$  and  $R$  are also known.

Most experimental observations of like-charge attraction fall in the regime of small and intermediate sized spheres ( $3 \lesssim \kappa R \lesssim 25$ ). Here we estimate that a long-range minimum in the interaction potential could be expected to occur at an intersurface separation of  $x_{\text{min}} \approx 5\kappa^{-1}$ . In experiments in water without any added salts,  $\kappa^{-1} \approx 100 - 200 \text{ nm}$ , implying the occurrence of minima in the pair potentials at intersurface separations in the range of  $0.5$  to  $1 \mu\text{m}$ . This is in good agreement with a range of experimental observations.<sup>9-12,14,15</sup> The proposed mechanism resolves the conundrum surrounding the appearance of an electrostatically governed long-ranged minimum in the interaction potential for a pair of like-charged particles in solution. The indication from this model is that

although the perturbation of electrical surface charge or potential at an object's surface is indeed infinitesimal at large interparticle separations, the integration of this miniscule change over a very large surface area (involving  $O(10^6)$  water molecules for the geometry considered) results in an overall non-negligible quantity and therefore ultimately in an observable effect. Furthermore, eqs 12 and 18 show that for  $\kappa R \gtrsim 1$ , to the first approximation, the magnitude of the attractive contribution, which can be seen to be reflected in the depth of the minimum in the pair potential, scales as the radius of the particle. This readily explains the experimental observation that larger particles ( $R = 3.25 \mu\text{m}$ ) present pair-potential minima of depths of around 3 to  $4k_{\text{B}}T$  and smaller particles ( $R = 0.65 \mu\text{m}$ ) are associated with much shallower minima of depths approximately 0.1 to  $0.5k_{\text{B}}T$ . We point out that whereas measurements involving smaller depths of the minimum in the pair potential ( $<0.5k_{\text{B}}T$ ) can be prone to conflation with imaging artifacts, experiments using larger particles are less vulnerable to these spurious effects. An additional point to note is that in the absence of any long-range attraction, the magnitude of the electrostatic free energy at intersurface separations corresponding to the location of the experimentally observed minima would generally be so high ( $O(300k_{\text{B}}T)$ ) as to render observation of particles at that separation impossible (Figure 2b, inset; red data series). This consideration alone would strongly hint at the presence of a long-range attraction counteracting the canonical repulsion in any experiment where particles can be observed to sample such separations. Such a characteristic is qualitatively different from an alternate scenario that might posit a weak attractive interaction that comes to the fore at interparticle separations where the electrostatic repulsion has turned negligible. Paying close attention to the exact parameters in specific experimental situations and performing a full calculation of the electrostatics permits us to glean important insight into key attributes of the underlying attraction. According to our picture, the shallow long-range minimum in the pair potential arises from the *near-total* cancellation of fairly substantial quantities (Figure 6a,c, inset).

We emphasize further that our rudimentary model for the free energy of the interfacial solvent is not expected to reflect the full experimental reality. This study highlights the fact that a small difference in the exact distance dependence of two essentially exponentially decaying free contributions is sufficient to generate a long-range minimum in the pair interaction potential. While the features of the pair potentials calculated based on this model capture important aspects of the experimental observations, the precise distance dependence of the solvent-governed long-range interaction free energy may change within a more comprehensive theoretical model combining electrostatics and interfacial solvation, and may turn even longer ranged than discussed here.

#### 4. CONCLUSIONS

To conclude, we summarize the mechanism underlying our proposed long-range force due to interfacial solvation. We also provide physical insight into how the behavior of interfacial solvent molecules, confined to within 0.5 nm of the surface, can, perhaps counterintuitively, drive an interaction that operates at very large distances ( $x \approx 10\kappa^{-1} \approx 1 \mu\text{m}$ ). In our model, the physical quantity coupling the behavior of interfacial solvent molecules to the electrostatics is  $\Delta\psi_s$ , the electrical potential perturbation on a particle surface due to the approach of another charged object. (See eq 10.) A change in  $\Delta\psi_s$  alters the

ionization state of the surface groups; the interfacial solvent molecules sense this change in charge state and respond by altering their average orientation. The response of the interfacial solvent entails a free-energy contribution,  $\Delta F_{\text{int}}$ , that is neglected within continuum theories. The fact that  $\Delta\psi_s$  can be nonzero at very large interparticle separations immediately implies that  $\Delta F_{\text{int}}$  can be correspondingly non-negligible. In other words, the interfacial solvation force we propose can be expected to be as long-ranged as the electrical influence exerted by one particle on another.

Our work suggests that Grier et al. correctly identified the biexponential nature of the total interaction potential in the like-charge attraction problem.<sup>11,30</sup> It is worth noting that the space charge invoked in their heuristic model generates an effect equivalent to that of a screened Coulombic attraction that decays at a rate corresponding to twice the Debye length. (See the Introduction.) The larger observed screening length for the attraction term, compared with the repulsion, is qualitatively in line with a key feature of the mechanism we propose, albeit for a completely different reason. Nonetheless, it is now evident that essentially the same functional form has been encountered in several independent experimental measurements of the interparticle potential, with widely different particle surface chemistries.<sup>9,11,14,15</sup> The precise origin of this feature finds explanation in our proposed mechanism that invokes the orientation of interfacial solvent molecules at a charge-regulating surface.

We note that a long-range minimum in the interaction potential arises as a special case when the attractive and repulsive terms balance each other at some distance. When this condition is not met, the total pair interaction energy is expected to be either attractive or repulsive at all separations. This feature of the model, in fact, ties in nicely with the experimental observation that charged particles are often observed to stick to like-charged surfaces in aqueous solution, even when substantial repulsions are nominally expected. In practice, owing to the lack of other general mechanisms for attraction, this sort of behavior, typically viewed through the lens of Derjaguin–Landau–Verwey–Overbeek (DLVO) theory, is inevitably attributed to attractive vdW forces.<sup>4,70</sup> Other possible explanations for such behavior include short-range hydration forces not explicitly related to surface charge<sup>71</sup> or potentially even an inversion in the sign of the charge of one of the interacting entities.<sup>38,58</sup> Note that even when a long-range minimum does occur for like-charged spherical particles, it does not preclude the occurrence of shorter range monotonic attraction-to-contact, separated from the “secondary” long-range minimum by a large free energy barrier, all governed by the same interfacial solvation mechanism (Figure 6c). Moreover, we emphasize that the presence of the long-range solvation-governed contribution does not automatically imply that the measured interaction between two negatively charged surfaces will appear net-attractive at all distances or that a minimum will be observed. In many cases,  $\Delta F_{\text{el}}$  will dominate  $|\Delta F_{\text{int}}|$  at all separations, and an exponentially decaying repulsion of lower magnitude—in apparent consonance with the DLVO expectation—is all that will be observed in experiment. In measurements involving colloidal particles and macroscopic surfaces, the use of fit parameters, for example, surface charge densities, can hinder the ability to tease apart contributions that decay or grow in a similar fashion, thus tending to mask more complex underlying behavior. This is likely to be less of a concern in interaction energy measurements

involving molecular scale probes whose geometry and composition can be very well defined.<sup>72</sup>

In general, the interfacial mechanism that we have described opens up the possibility of a strong, long-range, exponentially screened contribution to the total interaction energy between like-charged objects in solution, with a long-range minimum possible when additional conditions are met. Depending on the details of the problem at hand, namely, the sign of the surface charge on each particle, the composition of the ionizable chemical groups, the pH and pK in solution, the nature of the solvent molecule, and so on, this contribution from the molecular solvent may act to either augment or diminish the conventional electrostatic force, whether repulsive or attractive.

Interfacial water has long been known to play a major role in short-range hydration forces<sup>71,73–75</sup> and more broadly in the thermodynamics of molecular binding interactions.<sup>76,77</sup> Our results suggest that in the interaction of charged entities in solution, there very likely exists in addition a substantial *long-range* force due to the solvent. This mechanism may also play a role in the now widely observed tunable attraction involving charged macromolecules in solution<sup>78,79</sup> and in such apparently disparate experimental observations as the packaging of histone-coated chromosomal DNA in cells, the intracellular clustering of glycogen granules, crystallization, and pH-induced gelation. These are but a few instances in soft matter and molecular biology where entities carrying negative electrical charge spontaneously form clusters, often in a reversible manner depending on the solution conditions. Such behavior is indicative of a tunable attractive pairwise interaction that may well find its origins in the orientational behavior of water at the molecular interface in solution.

## AUTHOR INFORMATION

### Corresponding Author

**Madhavi Krishnan** – *Physical & Theoretical Chemistry Laboratory, Department of Chemistry, University of Oxford, Oxford OX1 3QZ, United Kingdom; Merton College, Oxford OX1 4JD, United Kingdom; [orcid.org/0000-0003-1274-7155](https://orcid.org/0000-0003-1274-7155); Email: [madhavi.krishnan@chem.ox.ac.uk](mailto:madhavi.krishnan@chem.ox.ac.uk)*

### Authors

**Ali Behjatian** – *Physical & Theoretical Chemistry Laboratory, Department of Chemistry, University of Oxford, Oxford OX1 3QZ, United Kingdom*

**Rowan Walker-Gibbons** – *Physical & Theoretical Chemistry Laboratory, Department of Chemistry, University of Oxford, Oxford OX1 3QZ, United Kingdom*

**Alexander A. Schekochihin** – *Rudolf Peierls Centre for Theoretical Physics, University of Oxford, Oxford OX1 3PU, United Kingdom; Merton College, Oxford OX1 4JD, United Kingdom*

Complete contact information is available at:

<https://pubs.acs.org/10.1021/acs.langmuir.1c02801>

### Notes

The authors declare no competing financial interest.

## ACKNOWLEDGMENTS

The authors gratefully acknowledge Dirk Aarts for providing expertise on Monte Carlo simulations. This project has received funding from the European Research Council (ERC) under the European Union's Horizon 2020 research and innovation programme (grant agreement no. 724180).

## REFERENCES

- (1) Sader, J. E.; Chan, D. Y. C. Long-range electrostatic attractions between identically charged particles in confined geometries: An unresolved problem. *J. Colloid Interface Sci.* **1999**, *213*, 268–269.
- (2) Netz, R. R. Electrostatics of counter-ions at and between planar charged walls: From Poisson-Boltzmann to the strong-coupling theory. *Eur. Phys. J. E: Soft Matter Biol. Phys.* **2001**, *5*, S57–S74.
- (3) Neu, J. C. Wall-mediated forces between like-charged bodies in an electrolyte. *Phys. Rev. Lett.* **1999**, *82*, 1072–1074.
- (4) Langmuir, I. The role of attractive and repulsive forces in the formation of tactoids, thixotropic gels, protein crystals and coacervates. *J. Chem. Phys.* **1938**, *6*, 873–896.
- (5) Klug, A.; Franklin, R. E.; Humphreysowen, S. P. F. The crystal structure of Tipula iridescent virus as determined by Bragg reflection of visible light. *Biochim. Biophys. Acta* **1959**, *32*, 203–219.
- (6) Luck, W. A. P.; Stranski, I. Kristallstrukturen aus nichtmolekularen Bausteinen. *Physikalische Blätter* **1967**, *23*, 304.
- (7) Kose, A.; Ozaki, M.; Takano, K.; Kobayashi, Y.; Hachisu, S. Direct observation of ordered latex suspension by metallurgical microscope. *J. Colloid Interface Sci.* **1973**, *44*, 330–338.
- (8) Williams, R.; Crandall, R. S.; Wojtowicz, P. J. Melting of crystalline suspensions of polystyrene spheres. *Phys. Rev. Lett.* **1976**, *37*, 348–351.
- (9) Kepler, G. M.; Fraden, S. Attractive potential between confined colloids at low ionic-strength. *Phys. Rev. Lett.* **1994**, *73*, 356–359.
- (10) Larsen, A. E.; Grier, D. G. Like-charge attractions in metastable colloidal crystallites. *Nature* **1997**, *385*, 230–233.
- (11) Grier, D. G.; Han, Y. Anomalous interactions in confined charge-stabilized colloid. *J. Phys.: Condens. Matter* **2004**, *16*, S4145–S4157.
- (12) Baksh, M. M.; Jaros, M.; Groves, J. T. Detection of molecular interactions at membrane surfaces through colloid phase transitions. *Nature* **2004**, *427*, 139–141.
- (13) Krishnan, M.; Monch, I.; Schulle, P. Spontaneous stretching of DNA in a two-dimensional nanoslit. *Nano Lett.* **2007**, *7*, 1270–1275.
- (14) Tata, B. V. R.; Mohanty, P. S.; Valsakumar, M. C. Bound pairs: Direct evidence for long-range attraction between like-charged colloids. *Solid State Commun.* **2008**, *147*, 360–365.
- (15) Gomez, E. W.; Clack, N. G.; Wu, H. J.; Groves, J. T. Like-charge interactions between colloidal particles are asymmetric with respect to sign. *Soft Matter* **2009**, *5*, 1931–1936.
- (16) Lin, P.-K.; Lin, K.-h.; Fu, C.-C.; Lee, K. C.; Wei, P.-K.; Pai, W.-W.; Tsao, P.-H.; Chen, Y. L.; Fann, W. S. One-Dimensional Dynamics and Transport of DNA Molecules in a Quasi-Two-Dimensional Nanoslit. *Macromolecules* **2009**, *42*, 1770–1774.
- (17) Musheev, M. U.; Kanoatov, M.; Retif, C.; Krylov, S. N. Stable DNA Aggregation by Removal of Counterions. *Anal. Chem.* **2013**, *85*, 10004–10007.
- (18) Winter, E. M.; Groves, J. T. Surface binding affinity measurements from order transitions of lipid membrane-coated colloidal particles. *Anal. Chem.* **2006**, *78*, 174–180.
- (19) Kardar, M.; Golestanian, R. The “friction” of vacuum, and other fluctuation-induced forces. *Rev. Mod. Phys.* **1999**, *71*, 1233–1245.
- (20) Trizac, E.; Raimbault, J. L. Long-range electrostatic interactions between like-charged colloids: Steric and confinement effects. *Phys. Rev. E: Stat. Phys., Plasmas, Fluids, Relat. Interdiscip. Top.* **1999**, *60*, 6530–6533.
- (21) Belloni, L. Colloidal interactions. *J. Phys.: Condens. Matter* **2000**, *12*, R549–R587.
- (22) Crocker, J. C.; Grier, D. G. When like charges attract: The effects of geometrical confinement on long-range colloidal interactions. *Phys. Rev. Lett.* **1996**, *77*, 1897–1900.
- (23) Grier, D. G. When like charges attract: interactions and dynamics in charge-stabilized colloidal suspensions. *J. Phys.: Condens. Matter* **2000**, *12*, A85–A94.
- (24) Baumgartl, J.; Arauz-Lara, J. L.; Bechinger, C. Like-charge attraction in confinement: myth or truth? *Soft Matter* **2006**, *2*, 631–635.
- (25) Baumgartl, J.; Bechinger, C. On the limits of digital video microscopy. *Europhys. Lett.* **2005**, *71*, 487–493.

- (26) Ise, N. Like likes like: counterion-mediated attraction in macroionic and colloidal interaction. *Phys. Chem. Chem. Phys.* **2010**, *12*, 10279–10287.
- (27) dos Santos, A. P.; Levin, Y. Like-Charge Attraction between Metal Nanoparticles in a 1:1 Electrolyte Solution. *Phys. Rev. Lett.* **2019**, *122*, 248005.
- (28) Bevan, M. A.; Prieve, D. C. Direct measurement of retarded van der Waals attraction. *Langmuir* **1999**, *15*, 7925–7936.
- (29) Han, Y.; Grier, D. G. Confinement-Induced Colloidal Attractions in Equilibrium. *Phys. Rev. Lett.* **2003**, *91*, 038–302.
- (30) Polin, M.; Grier, D. G.; Han, Y. Colloidal electrostatic interactions near a conducting surface. *Phys. Rev. E* **2007**, *76*, 041–406.
- (31) Kubincová, A.; Hünenberger, P. H.; Krishnan, M. Interfacial solvation can explain attraction between like-charged objects in aqueous solution. *J. Chem. Phys.* **2020**, *152*, 104713.
- (32) Reif, M. M.; Hunenberger, P. H. Origin of Asymmetric Solvation Effects for Ions in Water and Organic Solvents Investigated Using Molecular Dynamics Simulations: The Swain Acidity-Basicity Scale Revisited. *J. Phys. Chem. B* **2016**, *120*, 8485–8517.
- (33) Ye, S.; Nihonyanagi, S.; Uosaki, K. Sum frequency generation (SFG) study of the pH-dependent water structure on a fused quartz surface modified by an octadecyltrichlorosilane (OTS) monolayer. *Phys. Chem. Chem. Phys.* **2001**, *3*, 3463–3469.
- (34) Myalitsin, A.; Urashima, S.-h.; Nihonyanagi, S.; Yamaguchi, S.; Tahara, T. Water Structure at the Buried Silica/Aqueous Interface Studied by Heterodyne-Detected Vibrational Sum-Frequency Generation. *J. Phys. Chem. C* **2016**, *120*, 9357–9363.
- (35) Irudayam, S. J.; Henschman, R. H. Long-range hydrogen-bond structure in aqueous solutions and the vapor-water interface. *J. Chem. Phys.* **2012**, *137*, 034508.
- (36) Chen, Y. X.; Okur, H. I.; Gomopoulos, N.; Macias-Romero, C.; Cremer, P. S.; Petersen, P. B.; Tocci, G.; Wilkins, D. M.; Liang, C. W.; Ceriotti, M.; Roke, S. Electrolytes induce long-range orientational order and free energy changes in the H-bond network of bulk water. *Science Advances* **2016**, *2*, No. e1501891.
- (37) Sharp, K. A.; Honig, B. Calculating total electrostatic energies with the nonlinear Poisson-Boltzmann equation. *J. Phys. Chem.* **1990**, *94*, 7684–7692.
- (38) Theodoor, J.; Overbeek, G. The role of energy and entropy in the electrical double layer. *Colloids Surf.* **1990**, *51*, 61–75.
- (39) Biesheuvel, P. M. Electrostatic free energy of interacting ionizable double layers. *J. Colloid Interface Sci.* **2004**, *275*, 514–522.
- (40) Ninham, B. W.; Parsegian, V. A. Electrostatic potential between surfaces bearing ionizable groups in ionic equilibrium with physiologic saline solution. *J. Theor. Biol.* **1971**, *31*, 405–428.
- (41) Pericet-Camara, R.; Papastavrou, G.; Behrens, S. H.; Borkovec, M. Interaction between charged surfaces on the Poisson-Boltzmann level: The constant regulation approximation. *J. Phys. Chem. B* **2004**, *108*, 19467–19475.
- (42) Popa, I.; Sinha, P.; Finessi, M.; Maroni, P.; Papastavrou, G.; Borkovec, M. Importance of Charge Regulation in Attractive Double-Layer Forces between Dissimilar Surfaces. *Phys. Rev. Lett.* **2010**, *104*, 228–301.
- (43) Macias-Romero, C.; Nahalka, I.; Okur, H. I.; Roke, S. Optical imaging of surface chemistry and dynamics in confinement. *Science* **2017**, *357*, 784–787.
- (44) Ong, S. W.; Zhao, X. L.; Eisenthal, K. B. Polarization of water molecules at a charged interface - 2nd harmonic studies of the silica water interface. *Chem. Phys. Lett.* **1992**, *191*, 327–335.
- (45) Bonthuis, D. J.; Gekle, S.; Netz, R. R. Profile of the Static Permittivity Tensor of Water at Interfaces: Consequences for Capacitance, Hydration Interaction and Ion Adsorption. *Langmuir* **2012**, *28*, 7679–7694.
- (46) Mamatkulov, S. I.; Allolio, C.; Netz, R. R.; Bonthuis, D. J. Orientation-Induced Adsorption of Hydrated Protons at the Air-Water Interface. *Angew. Chem., Int. Ed.* **2017**, *56*, 15846–15851.
- (47) Latimer, W. M.; Pitzer, K. S.; Slansky, C. M. The free energy of hydration of gaseous ions, and the absolute potential of the normal calomel electrode. *J. Chem. Phys.* **1939**, *7*, 108–111.
- (48) Roux, B.; Yu, H. A.; Karplus, M. Molecular-basis for the Born model of ion solvation. *J. Phys. Chem.* **1990**, *94*, 4683–4688.
- (49) Babu, C. S.; Lim, C. Theory of ionic hydration: Insights from molecular dynamics simulations and experiment. *J. Phys. Chem. B* **1999**, *103*, 7958–7968.
- (50) Skelton, A. A.; Fenter, P.; Kubicki, J. D.; Wesolowski, D. J.; Cummings, P. T. Simulations of the Quartz(10(1)over-bar1)/Water Interface: A Comparison of Classical Force Fields, Ab Initio Molecular Dynamics, and X-ray Reflectivity Experiments. *J. Phys. Chem. C* **2011**, *115*, 2076–2088.
- (51) Quezada, G. R.; Rozas, R. E.; Toledo, P. G. Molecular Dynamics Simulations of Quartz (101)-Water and Corundum (001)-Water Interfaces: Effect of Surface Charge and Ions on Cation Adsorption, Water Orientation, and Surface Charge Reversal. *J. Phys. Chem. C* **2017**, *121*, 25271–25282.
- (52) Muntean, S. A.; Gerasimov, R. A.; Lyulin, A. V. Dynamics of Water Near Oxidized Polystyrene Films. *Macromol. Theory Simul.* **2012**, *21*, 544–552.
- (53) Kathmann, S. M.; Kuo, I. F. W.; Mundy, C. J.; Schenter, G. K. Understanding the Surface Potential of Water. *J. Phys. Chem. B* **2011**, *115*, 4369–4377.
- (54) Leung, K. Surface Potential at the Air-Water Interface Computed Using Density Functional Theory. *J. Phys. Chem. Lett.* **2010**, *1*, 496–499.
- (55) Paluch, M. Electrical properties of free surface of water and aqueous solutions. *Adv. Colloid Interface Sci.* **2000**, *84*, 27–45.
- (56) Kathmann, S. M.; Kuo, I. F. W.; Mundy, C. J. Electronic Effects on the Surface Potential at the Vapor-Liquid Interface of Water. *J. Am. Chem. Soc.* **2008**, *130*, 16556–16561.
- (57) Kastenholtz, M. A.; Hunenberger, P. H. Computation of methodology-independent ionic solvation free energies from molecular simulations. I. The electrostatic potential in molecular liquids. *J. Chem. Phys.* **2006**, *124*, 124106.
- (58) Carnie, S. L.; Chan, D. Y. C.; Gunning, J. S. Electrical double-layer interaction between dissimilar spherical colloidal particles and between a sphere and a plate - the linearized Poisson Boltzmann theory. *Langmuir* **1994**, *10*, 2993–3009.
- (59) Brunner, M.; Dobnikar, J.; von Grunberg, H. H.; Bechinger, C. Direct measurement of three-body interactions amongst charged colloids. *Phys. Rev. Lett.* **2004**, *92*, 078301.
- (60) Tsui, F. C.; Ojcius, D. M.; Hubbell, W. L. The intrinsic pKa values for Phosphatidylserine and Phosphatidylethanolamine in Phosphatidylcholine host bilayers. *Biophys. J.* **1986**, *49*, 459–468.
- (61) Dong, H. T.; Du, H. B.; Wickramasinghe, S. R.; Qian, X. H. The Effects of Chemical Substitution and Polymerization on the pK(a) Values of Sulfonic Acids. *J. Phys. Chem. B* **2009**, *113*, 14094–14101.
- (62) Darlington, A. M.; Gibbs-Davis, J. M. Bimodal or Trimodal? The Influence of Starting pH on Site Identity and Distribution at the Low Salt Aqueous/Silica Interface. *J. Phys. Chem. C* **2015**, *119*, 16560–16567.
- (63) Vishnyakov, A.; Li, T.; Neimark, A. V. Adhesion of Phospholipid Bilayers to Hydroxylated Silica: Existence of Nanometer-Thick Water Interlayers. *Langmuir* **2017**, *33*, 13148–13156.
- (64) Stern, H. O. Zur Theorie der Elektrolytischen Doppelschicht. *Zeitschrift für Elektrochemie und angewandte physikalische Chemie* **1924**, *30*, 508–516.
- (65) Levine, S.; Dube, G. P. Interaction between two hydrophobic colloidal particles, using the approximate Debye-Hückel theory. I. General properties. *Trans. Faraday Soc.* **1939**, *35*, 1125–1140.
- (66) Glendinning, A.; Russel, W. The electrostatic repulsion between charged spheres from exact solutions to the linearized poisson-boltzmann equation. *J. Colloid Interface Sci.* **1983**, *93*, 95–104.
- (67) Bell, G.; Levine, S.; McCartney, L. Approximate methods of determining the double-layer free energy of interaction between two charged colloidal spheres. *J. Colloid Interface Sci.* **1970**, *33*, 335–359.
- (68) Krozel, J.; Saville, D. Electrostatic interactions between two spheres: Solutions of the debye-hückel equation with a charge regulation boundary condition. *J. Colloid Interface Sci.* **1992**, *150*, 365–373.

(69) Verwey, E. J. W.; Overbeek, J. T. G.; van Nes, K. *Theory of the Stability of Lyophobic Colloids: The Interaction of Sol Particles Having an Electric Double Layer*; Elsevier Publishing Company, 1948; pp 37–40.

(70) Hartley, P. G.; Larson, I.; Scales, P. J. Electrokinetic and direct force measurements between silica and mica surfaces in dilute electrolyte solutions. *Langmuir* **1997**, *13*, 2207–2214.

(71) Israelachvili, J.; Wennerstrom, H. Role of hydration and water structure in biological and colloidal interactions. *Nature* **1996**, *379*, 219–225.

(72) Ruggeri, F.; Zosel, F.; Mutter, N.; Rozycka, M.; Wojtas, M.; Ozyhar, A.; Schuler, B.; Krishnan, M. Single-molecule electrometry. *Nat. Nanotechnol.* **2017**, *12*, 488–495.

(73) Parsegian, V. A.; Fuller, N.; Rand, R. P. Measured work of deformation and repulsion of lecithin bilayers. *Proc. Natl. Acad. Sci. U. S. A.* **1979**, *76*, 2750–2754.

(74) Israelachvili, J. N.; Pashley, R. M. Molecular layering of water at surfaces and origin of repulsive hydration forces. *Nature* **1983**, *306*, 249–250.

(75) Schlaich, A.; dos Santos, A. P.; Netz, R. R. Simulations of Nanoseparated Charged Surfaces Reveal Charge-Induced Water Reorientation and Nonadditivity of Hydration and Mean-Field Electrostatic Repulsion. *Langmuir* **2019**, *35*, 551–560.

(76) Dunitz, J. D. The entropic cost of bound water in crystals and biomolecules. *Science* **1994**, *264*, 670–670.

(77) Ladbury, J. E. Just add water! The effect of water on the specificity of protein-ligand binding sites and its potential application to drug design. *Chem. Biol.* **1996**, *3*, 973–980.

(78) Franzmann, T. M.; Jahnel, M.; Pozniakovsky, A.; Mahamid, J.; Holehouse, A. S.; Nuske, E.; Richter, D.; Baumeister, W.; Grill, S. W.; Pappu, R. V.; Hyman, A. A.; Alberti, S. Phase separation of a yeast prion protein promotes cellular fitness. *Science* **2018**, *359*, No. eaao5654.

(79) Maharana, S.; et al. RNA buffers the phase separation behavior of prion-like RNA binding proteins. *Science* **2018**, *360*, 918–921.

## Recommended by ACS

### Charge Transport in Water–NaCl Electrolytes with Molecular Dynamics Simulations

Øystein Gullbrekken, Sondre Kvalvåg Schnell, *et al.*

MARCH 15, 2023

THE JOURNAL OF PHYSICAL CHEMISTRY B

[READ](#)

### Theory of Charge Regulation of Colloidal Particles in Electrolyte Solutions

Amin Bakhshandeh, Yan Levin, *et al.*

NOVEMBER 01, 2022

LANGMUIR

[READ](#)

### Connecting Colloidal Forces to the Equilibrium Thickness of Particulate Deposits on a Substrate in Contact with a Suspension Using Classical Density Functional Theory

Roi Bar-On and Ofer Manor

APRIL 10, 2023

LANGMUIR

[READ](#)

### Colloidal Suspensions Displaying Anomalous Phoretic Behavior: Field and Mobility Reversal

Vincenzo Tricoli and Fulvio F. Corinaldesi

SEPTEMBER 06, 2022

LANGMUIR

[READ](#)

[Get More Suggestions >](#)